University of Alberta

The Essential Work of Fracture Method Applied to Mode II Interlaminar Fracture in Fiber Reinforced Polymers

by

Scott David McKinney

A thesis submitted to the Faculty of Graduate Studies and Research
in partial fulfillment of the requirements for the degree of

Master of Science

Mechanical Engineering

Spring 2013
Edmonton, Alberta

Abstract

This thesis presents a new method for determining mode II interlaminar fracture toughness in fiber reinforced polymers (FRP) using the essential work of fracture (EWF) method. Fracture tests were performed on a tabbed double edge notched shear (DENS) specimen, made from a unidirectional glass/epoxy laminate, in an Iosipescu fixture. The EWF in mode II was found to agree with the G_{IIc} for fracture initiation value from an ENF test.

A finite element model was used to determine mechanisms involved in the DENS specimen. Interlaminar fracture was simulated using cohesive elements and the unstable crack growth path was simulated using the Riks arc length method. The numerical results closely match the empirical results. The model reveals that even though the EWF could be found using the conventional linear extrapolation, elastic strain energy, rather than the usual plastic energy, is the dominant geometry dependent property.

Acknowledgements

I want to thank my supervisor Dr. Ben Jar for his guidance, patience, and financial support throughout my studies.

I also wish to show my appreciation to my colleagues in the Failure Analysis and Materials Evaluation Group for their discussion, feedback, and friendship: Tsegay Belay, Souvenir Muhammad, Zhaowui Yang, Kevin Brethome, and Feng Yu.

Finally I extend gratitude to my parents, Janet and Paul McKinney. I thank them for their support and their unwavering confidence in me.

Table of Contents

Chapter 1 - Introduction 1

Objectives 1

Uses of Composite Materials 1

Background 2

Iosipescu Fixture 4

Iosipescu Test of Composites and Adhesives 5

Essential Work of Fracture (EWF) Method 7

Overview of the Present Study 9

Chapter 2 - Methodology 10

Introduction 10

Empirical Methods 10

FRP Panels 10

Double Edge Notched Shear (DENS) Specimen 11

Edge Notched Flexure (ENF) Specimen 11

Iosipescu Test Procedure 12

ENF Procedure 13

Material Characterization 14

Scattering Control 15

Finite Element Model 16

Idealized Geometry 16

FEM Construction 16

Hill Plasticity Model 20

Cohesive Elements 21

The Riks Arc Length Method 23

Virtual Experiment in FEM 24

FEM Validation with Uncracked Specimen 24

Chapter 3 - Results 25
Introduction 25
Material Characterization 25
Iosipescu DENS Results 26
ENF Results 31
Model Validation 33
Finite Element Results 35
Chapter 4 - Discussion 44
Introduction 44
Empirical Results 44
FEM Results 45
EWF Applied to Iosipescu DENS 46
Comparison to Other Tests 46
Arc Length Methods 48
Cohesive Elements 49
Compliant Tab Interface 50
Chapter 5 - Conclusions and Future Study 52
Conclusions 52
Future Study 53
References 54

List of Tables

Table 2.1: Elastic Properties..... 19

Table 2.2: Hill Coefficients 20

Table 3.1: Properties of Inspected Samples 26

Table 3.2: Stiffness of the DENS Samples 28

Table 3.3: Stiffness of Model Sections..... 33

Table 3.4: Relative Energy Content of DENS Specimen at Maximum Load..... 37

List of Figures

Figure 1.1: Structure of a Laminated Composite Panel 3
Figure 1.2: Crack Separation Modes 3
Figure 1.3: The Modified Wyoming Iosipescu Fixture 5
Figure 1.4: A Typical Iosipescu Failure 6
Figure 1.5: Energy Partition for EWF in DENT Specimen 7
Figure 1.6: DENS Specimen Used for Mode II EWF in Polymers 9

Figure 2.1: Iosipescu DENS Specimen 12
Figure 2.2: ENF Specimen 12
Figure 2.3: Tabbed DENS Sample in Positioner Jig 13
Figure 2.4: Idealized Geometry 16
Figure 2.5: Finite Element Model of the Iosipescu DENS Test 18
Figure 2.6: Model of the DENS specimen 18
Figure 2.7: Resin Rich Response 19
Figure 2.8: Softening of Cohesive Elements 22
Figure 2.9: The Riks Method 23

Figure 3.1: Microstructure of the DENS Specimen 25
Figure 3.2: A Typical Iosipescu DENS test 27
Figure 3.3: Specific Work of Fracture in all Ligament Lengths 27
Figure 3.4: Iosipescu Fracture Surfaces 28
Figure 3.5: Fibers in the Ligament Area 28
Figure 3.6: Peak Load of Iosipescu DENS Test 29
Figure 3.7: Fracture Displacement of Iosipescu DENS Test 29
Figure 3.8: Thickness Independence of Peak Loads 30
Figure 3.9: Thickness Independence of Fracture Displacements 30
Figure 3.10: Normalized Results from the IDENS Test 31
Figure 3.11: A Typical ENF Test 32
Figure 3.12: Iosipescu DENS Compared to ENF 32
Figure 3.13: Maximum Force in FE Model 33
Figure 3.14: Breaking Displacement in FEM 34
Figure 3.15: Maximum Nominal Stress in FEM 34
Figure 3.16: Test of Uncracked Specimen 35
Figure 3.17: Virtual Experiment 36
Figure 3.18: EWF of Virtual Iosipescu DENS 36
Figure 3.19: Plastic Shear Strain in 4mm 38
Figure 3.20: Strain Energy Density in 4mm 39
Figure 3.21: Contact Pressure From the Iosipescu Fixture 40
Figure 3.22: Virtual Test of the 5mm Iosipescu DENS 41
Figure 3.23: Ligament Shear Stress 42
Figure 3.24: Ligament Normal Stress 42
Figure 3.25: Damage Propagation 43
Figure 3.26: Transition to Stable Fracture 43

Chapter 1 - Introduction

Objectives

The objective of this thesis is to investigate the possibility of using the essential work of fracture (EWF) method to characterize the mode II (sliding mode) interlaminar fracture toughness in fiber reinforced polymers (FRP). A new fracture toughness test, the Iosipescu double edge notched shear (IDENS) test, has been created for interlaminar fracture testing. Specimens were tested using a Modified Wyoming Iosipescu fixture. The Iosipescu test fixture was chosen because it applies a direct shear load. There is currently no international standard for a mode II interlaminar fracture toughness test. Using the EWF method with a double edge notched shear specimen (DENS) in an Iosipescu fixture is presented as an alternative to the existing methods for interlaminar fracture toughness.

The specific project objectives are:

1) Identify how the specific work of fracture scales with DENS ligament length

2) Validate the Iosipescu DENS test against an existing mode II fracture test

3) Determine the mechanisms of observed test behavior using a finite element model

4) Evaluate the success of the IDENS test for interlaminar fracture toughness

Uses of Composite Materials

While composite materials were once the exclusive domain of the aerospace industry, their use and influence is now ubiquitous. Composite materials are much cheaper than they once were which has motivated their development for a wide range of industrial and commercial applications. They are typically used to create lightweight structural shell members since FRP fabrication techniques favor thin composites.

A popular industrial application of composites is the construction of pressure vessels because filament winding allows precise control of the fiber angle, and thus optimization of the strong direction. A composite pressure vessel will either be entirely FRP, or wrapped around a metal base shell. Another industrial use that is improved by composite materials is windmill power plants. Laminated composite blades are much lighter than metal alternatives, thus reducing their structural requirements. Imbedded sensors are another appealing ability for industrial composites. FRP composites usually have a layered design which allows a sensor to be added during their fabrication. Laminated composite panels are also used to strengthen existing structures such as concrete beams. This is used for general reinforcement as well as repairs.

Common commercial applications include cars and sports equipment. Cars have used composites for specific components such as drive shafts for a long time. As their price has fallen, composites have entered into other areas as automotive manufacturers have tried to reduce vehicle weights. Structural components such as the vehicle frame are starting to be made of carbon fiber and fibreglass. Other common objects that are made of composites include hockey sticks, surf boards, fishing rods, tennis rackets, computer cases, golf clubs, and tent poles. FRP are also popular for marine applications because they don't rust. Small boats, such as canoes, are frequently made from fibreglass to reduce their weight.

Background

Laminated FRP are composed of multiple layers of individual lamina. A lamina is typically a unidirectional orientation of fiber bundles, such as what was studied here, or a woven bidirectional mat. An individual lamina is either a thin layer of reinforcement fibers preimpregnated with matrix resin or as in this work, a layer of fiber bundles stitched together with thread. Figure 1.1 is a schematic for the built up structure of a laminated composite panel.

A great advantage of FRP over other materials is the ability to tailor their properties for a specific application by controlling the orientation of the lamina that make up the complete laminate. A second advantage of laminated composites is that interlaminar devices are easy to add during the layup process. A potential application of interlaminar devices is structural health monitoring and inspection. Hautamaki et al [1] demonstrated that embedded, wireless strain sensors could be used for damage detection in an FRP Laminate. Another study done by Ratcliffe et al. [2] showed that a fast and accurate inspection could be performed using surface mounted accelerometers by tracking the dynamic response of a stabilizer from an Airbus A320 aircraft. Fiber optics have also emerged as a interlaminar devices for damage detection [3]. All Interlaminar devices can be considered interlaminar starter defects that create stress concentrations, thus making interlaminar fracture toughness even more important to understand clearly.

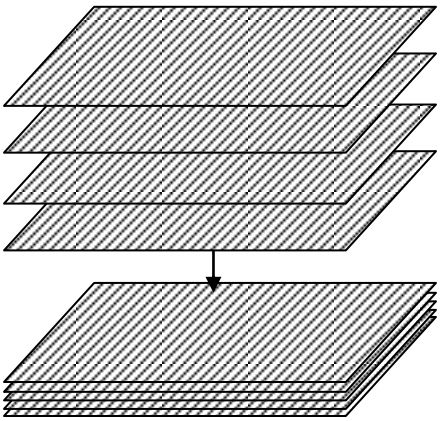

Figure 1.1: Structure of a Laminated Composite Panel

Although the in plane properties of a composite laminate can be easily adjusted, the interlaminar regions are much more difficult to strengthen. Interlaminar regions are matrix rich, with lower fiber content than the in plane regions, making their properties dominated by an isotropic material. Although attempts have been made to increase interlaminar toughness by stitching the layers together [4, 5] or adding support structures [6], in general the only option is to use a tougher matrix.

Interlaminar cracks reduce the stiffness and fatigue life of composite materials and introduce more buckling failure modes. Composite structures are difficult to repair and damage is difficult to detect so their fracture toughness must be well understood to predict stability and service life. Cracks grow under three separation modes which are demonstrated in Figure 1.2. Mode I (opening mode) occurs due to a tensile stress normal to the plane of the crack. Mode II (sliding mode) occurs due to a shear stress perpendicular to the crack front. Mode III (tearing mode) occurs due to a shear stress parallel to the crack front.

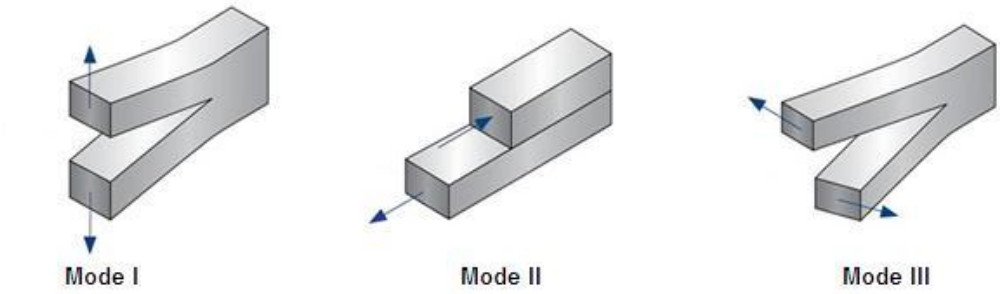

Figure 1.2: Crack Separation Modes

Mode II Interlaminar fracture occurs in laminated FRP because crack growth is confined by the adjacent fiber layers. Even though the matrix has been shown to crack in mode I at the microscopic scale [7], it is still considered a mode II fracture when studied as a macroscopic process.

Mode I interlaminar toughness is tested using the double cantilever beam test according to ISO Standard 15024 [8]. There are multiple Mode II tests that have been considered for standardization, but none has been adopted by the ISO [9, 10]. The lack of an international standard is partially due to disagreement among regional standards organizations as to which mode II test is the best, with the ASTM, ESIS, and JIS each championing a different one. O'Brien has published an explanation of this disagreement [9]. These organizations have different mandates, and different scopes of practice, which often leads to conflict.

Mode III is also not standardized, in this case because of difficulty of generating mode III separation.

Iosipescu Fixture

The Iosipescu shear fixture is named after its creator and appeared in the Journal of Metals in 1967 [11]. The test method was originally for testing the shear strength of metals but the fixture and the test have been adapted since then to test FRP and adhesives.

The original version of the Iosipescu fixture was two halves of a rectangular block with a rectangular specimen chamber. The specimen chamber was a fixed size and held samples in place with a screw on either side. One side remained fixed while a load was applied downward on the moving side. A newer version of the Iosipescu, the Wyoming configuration, was introduced for use on composite materials by Walrath and Adams, at the University of Wyoming, wherein they changed the box design to a four point contact [12]. The new contact pattern was to make it easier to insert specimens and it held them in place with a removable front face that included front mounted screws. Their work was the basis for the original ASTM standard D5379 in 1993.

The design in [12] was criticized by Conant and Odom for not restraining specimens against out of plane movement as well as for its susceptibility to a specimen twisting during a test [13]. Twisting was shown to lead to poor repeatability when subjected to a round robin test. They designed a series of alternatives before finally recommending one that solved both of these problems. Their major improvement was mounting both halves of the fixture to slider bars that prevented out of plane motion. They also added movable wedges that gave the specimen chamber an adjustable height.

The modern version of this test fixture is commonly referred to as the Modified Wyoming configuration and is seen in Figure 1.3. Adams and Walrath revisited

their design in 1986 to make it easier to use and to provide more accurate results [14]. Among their concerns were the small size of their original fixture, the proximity of load points to the gauge section, the requirement for precise dimensions (fixed size specimen bay), and a lack of specimen visibility while testing. The current ASTM standard uses the modified Wyoming configuration [15].

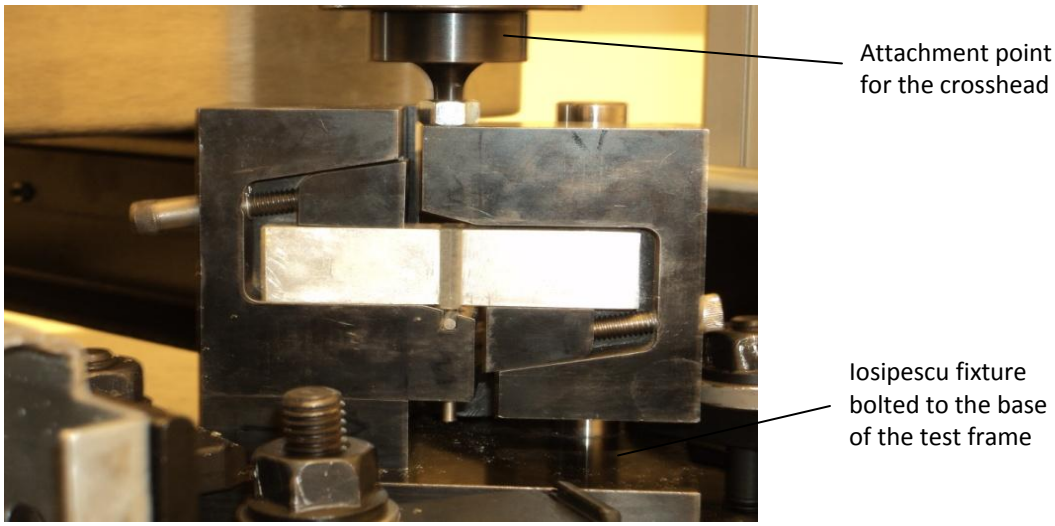

Figure 1.3: The Modified Wyoming Iosipescu Fixture

Iosipescu Test of Composites and Adhesives

The common Iosipescu test is used for determining the shear strength of FRP performed with a double V-notched beam specimen. The beam originally had a 90° notch angle when introduced by Iosipescu in order to remove the stress concentration at the notch tip and create a uniform shear stress. For orthotropic materials such as composites, it has been shown that a higher notch angle is required to reduce (but not remove) the stress concentration [14]. For testing of adhesives, the V-notched beam specimen is cut in half such that it can be glued along its gauge length [16].

Iosipescu shear tests have traditionally been used for in plane shear strength [17, 18], however it has also been used to test out of plane shear strength [19]. While the current Iosipescu tests of composites are useful for comparison, they have been criticized for not generating a shear fracture. The typical failure pattern of the V-notched beam is crack growth along the fiber direction for composites or at a 45° angle from the gauge section in isotropic materials. These are tensile failures at the matrix-fiber interface or along the principal stress plane, not a shear failure along the gauge section. Crack growth along the fiber direction is illustrated in Figure 1.4.

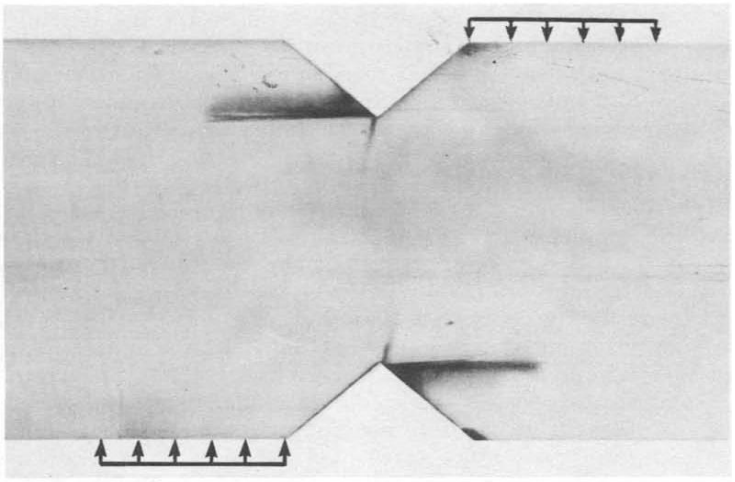

Figure 1.4: A Typical Iosipescu Failure [51]

To test out of plane shear properties, Gipple and Hoyns had to change the fiber orientation of the test specimen [19]. The new orientation was achieved by cutting their specimen from a thicker composite panel, which was built from 140 layers of S-Glass prepreg sheets. This allowed them to test the 2-3 material plane. Since this plane is isotropic, they observed the 45° failure angle along the principal stress planes. If the material direction was rotated 90° to apply an interlaminar shear stress, it would require a composite panel that is hundreds of layers thick. In principle, such a design could be used for interlaminar fracture toughness, but it is unlikely to be pursued.

In Chapter 3, it will be shown that the loads generated by the Iosipescu fixture are similar to an asymmetric four point beam. It is this property that is largely responsible for creating the shear dominated load in the center. This property holds as long as the specimen is stiff enough to resist bending and not deform excessively at the contact points. Others have used steel shims on the specimen surfaces to prevent local deformation and maintain the shear state [20]. Finite element analysis of the stress state created by the Iosipescu test has shown that although there is a stress concentration at the notch tips, the rest of the specimen is shear dominated and reasonably uniform [14, 21].

Adhesive testing is also conducted using the Iosipescu test. The V-notched beam is cut along its gauge length and glued back together to test the adhesive in a state of pure shear [22]. This allows stress-strain behavior to be measured.

Essential Work of Fracture (EWF) Method

EWF method was published in 1968 and was first performed on thin metal specimens [22]. It was later developed for polymers by Mai et al. [24]. This method is used mostly for determining Mode I fracture toughness.

The EWF method is an energy based technique for determining fracture toughness. The objective is to determine how much of the applied energy is consumed in forming a crack surface. The underlying principle behind this method is that energy is consumed in one of two ways. 1) Essential work of fracture is energy consumed by a new surface forming during crack growth. This energy mode will depend only on the size of the sample's ligament area and is independent of specimen geometry. 2) Non essential work of fracture is energy consumed by size and geometry dependent mechanisms. The mechanism of non essential work is usually plastic deformation energy. This principle is illustrated in Figure 1.5.

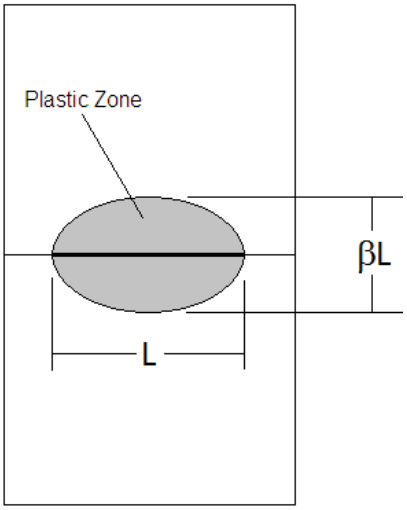

Figure 1.5: Energy Partition for EWF in DENT Specimen

Equations 1.1-1.3 show the simple application of this principle. Equation 1.2 separates the total energy into its intrinsic properties. The essential work of fracture (w_e) is per unit area while the geometry dependent/plastic energy (w_p) is expressed per unit volume. The essential work of fracture is determined from experiments by graphing the area specific work of fracture against multiple sample ligament lengths. Extrapolating the data back to a ligament length of 0 with Equation 1.3, theoretically removes the geometry dependent effects and gives the essential work of fracture.

$$W_f = W_e + W_p \qquad (1.1)$$

$$W_f = w_e \cdot L \cdot t + w_p \cdot \beta L \cdot L \cdot t \qquad (1.2)$$

$$w_f = w_e + \beta \cdot w_p \cdot L \qquad (1.3)$$

W_x - Work (kJ), x= f, e, p
w_f - Specific work of fracture (kJ/m^2)
w_e - Specific essential work of fracture (kJ/m^2)
w_p - Specific non essential work of fracture (kJ/m^3)
L - Ligament length (mm)
t - Specimen thickness (mm)
β - shape factor

Bárány et. al. summarized the conditions that must be met for an ideal EWF test [24, 25]: 1) There must be full ligament yielding prior to crack initiation, 2) The load displacement curves must be self similar, 3) A plane stress condition must dominate, and 4) The volume of the plastic dissipation must scale with the square of ligament length. The plane stress requirement is to prevent any significant change in the stress state during a test. One of the criticisms of the EWF method is that the fit line can result in a negative intercept (EWF). Bárány et. al. report that this is due to a change in stress state (plane stress to plane strain) or failure mode (ductile to brittle) of the sample during loading [24]. The plane strain problem is usually addressed through further energy partitioning [25]. Among the partitioning approaches are attempts to separate the energy used for necking, and energy used for ductile/brittle fractures. By contrast, the ideal condition of full ligament yielding is frequently not met [24].

The EWF method for mode II failure in polymers was demonstrated by Kwon and Jar for high density polyethylene (HDPE) and acrylonitrile butadiene styrene (ABS) using a Double Edge-Notched Shear (DENS) specimen. Their specimen, shown in Figure 1.6 was tested using an Iosipescu fixture. Their results suggest that mode II EWF has additional challenges when compared to mode I. During their tests of ABS, V-shaped grooves were added between the notch tips, on the sides of the specimen to prevent peeling [26]. The ligament area was adjusted by changing the depths of these grooves. Peeling was not a problem with HDPE wherein the ligament area was adjusted in the usual way, by adjusting its length [27]. This shows that extra effort may be required to prevent mode I failure in certain materials in order to test mode II.

Mode III EWF tests have been conducted using the trousers specimen in metals and polymers [24]. The extension into mode III has lead to additional energy partitioning strategies. In metals, a partition was introduced to remove the energy that causes bending [29]. In polymers, the fracture process zone has been split into moving initial and saturated (steady state) regions which follow the crack tip [29].

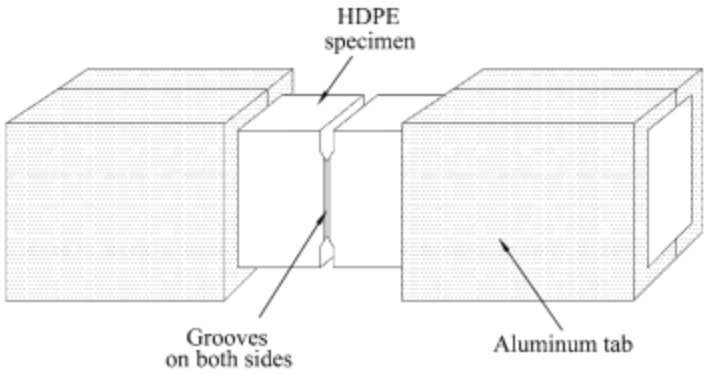

Figure 1.6: DENS Specimen Used for Mode II EWF in Polymers [27]

Overview of the Present Study

In the current chapter, modern uses for composite materials were introduced to show their relevance for study, followed by an introduction to mode II delamination in FRP. The Iosipescu test fixture and EWF data analysis method are presented and context is given for their use in fracture mechanics.

Chapter 2 presents the methods used in this work. The fabrication method for the glass/epoxy composite is explained, followed by test specimen descriptions and their testing and analysis procedures. The finite element model, which is used to investigate behavior mechanisms, is introduced in this chapter. Justification for an idealized 2D geometry is given, with the driving plasticity and cohesive zone models explained in context. The virtual experiment procedure also includes an explanation of the Riks arc length method, since it is a key step.

Chapter 3 will report the results of material evaluation, empirical tests, and numerical results. The finite element model is validated against empirical data in this chapter.

Chapter 4 will discuss the implication of the results from the IDENS test. The results and methods used in the present work will be then be compared to those used by others in the field of fracture mechanics.

Chapter 5 addresses the success of the IDENS test as a measure of interlaminar fracture toughness. What this work contributes to the field of fracture mechanics and potential directions for future work are also presented.

Chapter 2 - Methodology

Introduction

The objective of this chapter is to explain the materials, empirical procedures, and numerical procedures used in this work. For the empirical work, the material, specimens, test procedures, and analysis techniques are explained. For the numerical work using a finite element model, the idealized representation, material models, and solution techniques are explained. Brief explanations of standard test methods are given, while modifications to these methods and original methods are explained in detail. Particular attention is given to controlling data scatter.

Empirical Methods

FRP Panels

All test samples were cut from a unidirectional glass/epoxy panel. The panel was constructed using a hand layup technique and a vacuum chamber. A finished panel has dimensions 220mm x 220mm x 4.7mm.

A panel is made from 16 layers of e-glass fiber of two different fiber weights. The middle six layers are 9 oz/yd^2 (305.2 g/m^2) and the outer ten layers are 4.5 oz/yd^2 (152.6 g/m^2). The resin system used for the matrix is bisphenol-A epoxy and polyamine with commercial names Epon 826 and Epikure 9551, respectively provided by Momentive. The resin to hardener ratio is 100:36 by weight, which is recommended by the manufacturer.

The two different fibers were chosen because the stitching threads of the heavier fiber were easier to remove than the lighter fiber. Stitching threads were removed from the panel in the sample regions, in the middle six layers to prevent them from affecting crack initiation and propagation. Aluminum foil was used as a starter film to create a 20 μm thick interlaminar crack between the middle layers of the panel on both the DENS and ENF specimens. The foil was cut with a new razor blade and the foil edges were flattened before it was included in the laminate, to create a sharp crack tip.

Panels were created using a steel photo frame mold, which is clamped shut during the cure process. Fiber layup was done by adding one layer at a time and using a hand roller to ensure complete fiber wetting. To minimize the trapped air, a vacuum chamber was used to degas the epoxy resin after it was mixed. A vacuum stage was also used on the first eight layers of the panel, before adding the starter film, and on the completed sixteen layers, before the mold was closed. A vacuum pressure of 25 wg (6.22 kPa) below atmospheric was held for 30 minutes at each vacuum stage. The finished panel was cured at 50°C for 2 hours with a second stage at 120°C for 2.5 hours. The panel was cooled,

overnight to room temperature in the oven before being removed from the mold. This curing and cooling procedure is the one used by Hu, Xia, and Ellyin for the same resin system [28].

Samples were cut with diamond tipped abrasive saws. Roughing cuts were made using a tile saw, while finishing cuts were made with a low speed (60 rpm) saw. Cracks were opened by gently inserting a razor blade into the starter film. The low speed saw was used after the cracks were opened to prevent damage.

Double Edge Notched Shear (DENS) Specimen

The DENS specimen used in this work is based on the design Kwon and Jar [26] used to adapt the EWF technique to polymers in shear mode. The specimen in Figure 2.1 is the version which has been adapted for FRP. This specimen has symmetric, interlaminar edge cracks on either side of a ligament area. Each specimen is 21 mm tall and 14 mm wide, with ligament lengths (L) of 2 mm to 6 mm. Shear force is applied at the surfaces, parallel to the 1-2 material. Dimensions and material directions for the DENS are identified in

Figure 2.1: Iosipescu DENS Specimen

. Shear is applied through aluminum tabs which are glued onto the sides of the sample.

After the finishing cut, the final shape was reached using dry sandpaper. The symmetry of the sample was controlled as well as its final dimensions. To prevent surface stress concentrations from affecting test results, the sides with crack tips were polished with 500 grit (CAMI) sandpaper.

Edge Notched Flexure (ENF) Specimen

The ENF Specimen used in this work conforms to the European Structural Integrity Society Protocol for Interlaminar Fracture Testing of Composites [29]. The dimensions used in this work are displayed in Figure 2.2. The starter film thickness is 20 μm, rather than the protocol's recommendation of 15 μm or less. The thicker film was used to prevent it from wrinkling in the mold. The ENF specimen has a nominal width of 20 mm.

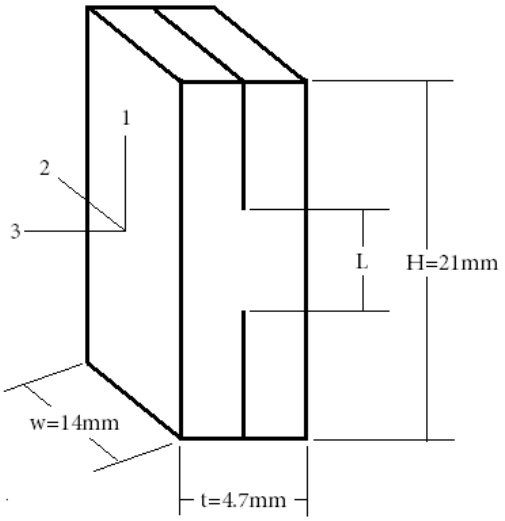

Figure 2.1: Iosipescu DENS Specimen

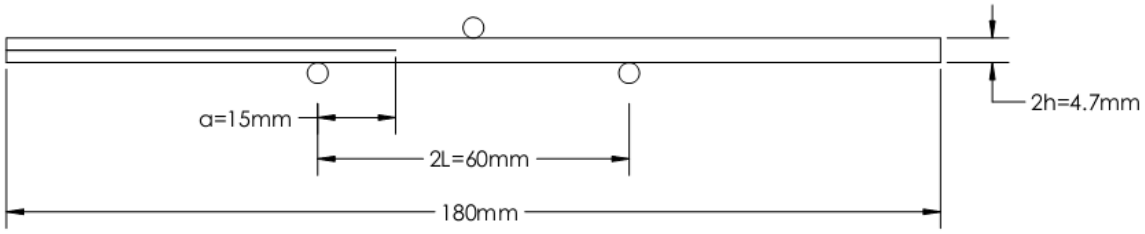

Figure 2.2: ENF Specimen

Iosipescu Test Procedure

DENS samples were mounted to aluminum tabs to fit in the Iosipescu fixture. The tabs are 20 mm x 12mm x 40 mm and bonded to the sample with DP460, a 3M adhesive used for joining metal to plastic. Sample edges were covered with tape to prevent the glue from contaminating the crack surface. The adhesive was cured at room temperature for 20 hours before testing. To prevent tab misalignments from introducing bending, all the samples were mounted using the positioner jig in Figure 2.3. A total of 41 DENS samples were tested.

Specimens were tested in an Iosipescu fixture, which is seen in Figure 1.3. The tab in the fixed side (left) was clamped first, then the moving side (right) tab was slowly clamped as the crosshead descended to prevent excessive load from being applied. For the 2 mm and 3 mm ligament lengths, Kopr Kote anti-seizing compound was applied to the tab surfaces to prevent friction from adding mode I loading.

Tests were conducted with a Galdabini Quasar 100 universal testing machine under displacement control at a constant crosshead speed of 1 mm/min. The applied force was measured by the machine's load cell and the displacement was assumed to be the crosshead stroke. Loading continued until the sample was broken.

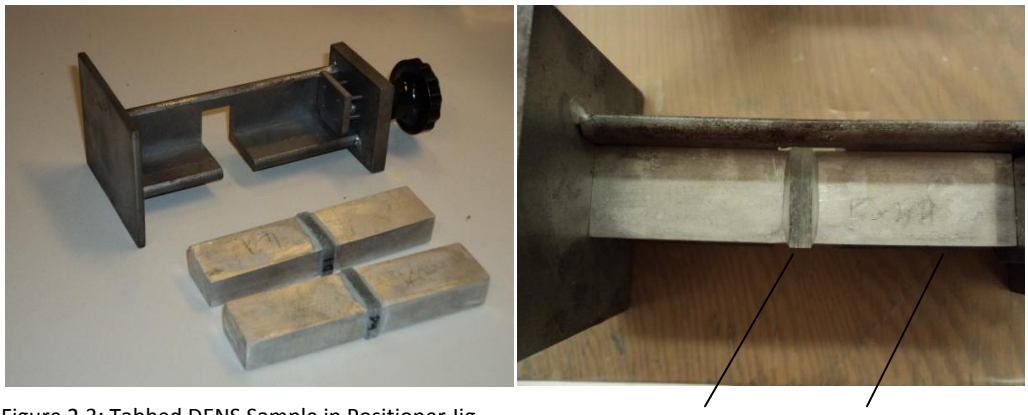

Figure 2.3: Tabbed DENS Sample in Positioner Jig

ENF Procedure

ENF Tests were conducted using a three point bending fixture. A span length of 60 mm was chosen to prevent large deformation, as required by the protocol. The crack length was 15 mm, which is the recommended one-quarter span length. A 1 mm/min crosshead speed was used for ENF tests and 6 samples were tested.

The critical energy release rate is calculated using equation 2.1, which is the beam theory formulation from the test protocol [29]. The equations parameters are illustrated in Figure 2.2.

$$G_{IIc} = \frac{9a^2 P\delta}{2B(2L^3 + 3a^3)} \qquad (2.1)$$

G_{IIc} - Critical strain energy release rate (kJ/m^2)
a - Crack length (mm)
P - Force at midpoint (N)
δ - Midpoint deflection (mm)
B - Beam width (mm)
L - Half span length (mm)

Three different measures of the energy release rate were calculated by using points specified in the test protocol [29]. These points are the nonlinear point, the 5% offset point, and the maximum load point. All three of these measures are used in the literature. The nonlinear point was determined by fitting a least squares regression line to the linear region of the force-displacement curve. The nonlinear point was chosen to be the point at which the force was 1% lower than the regression line. The 5% offset point is the intersection of the original force curve with a line corresponding to a 5% increase of the initial compliance.

Material Characterization

Two methods were used to determine the fiber volume fraction. The first method is a modified ASTM standard. The second method is microscopy.

Equation 2.2 is a method from ASTM D3171 for calculating the fiber volume fraction of a composite panel based on the weight of the fiber layers it's made from [30]. The ASTM method uses the area density of the fiber layers and the finished panel thickness to determine fiber volume fraction. The 10 in the denominator is due to the parameters' units that are used in the standard. The standard method has been adapted to consider the presence of two fiber weights. The outer 10 layers of the panel are labeled Fiber A and the inner 6 layers are labeled Fiber B. Equation 2.3 gives the average volume fraction by considering these layers' individual contributions to the finished panel. Equation 2.4 gives the local volume fraction for each fiber weight by considering them to be isolated sub laminates.

$$V = \frac{AN}{10\rho_r h} \quad (2.2)$$

$$V = \frac{A_a N_a + A_b N_b}{10\rho_r (h_a + h_b)} \quad (2.3)$$

$$V_a = \frac{A_a N_a}{10\rho_r h_a} \quad (2.4)$$

V - Fiber volume fraction
A - Glass area density (g/m^2)
N - Number of fiber layers
ρ_r - Density of reinforcement material (g/cm^3)
h - Panel thickness (cm)
h_x - Thickness of panel occupied by fiber type (cm), x= a or b

Fiber volume fraction was also determined using microscopy. Samples were cut through their ligament area, normal to the fiber direction and photographed under high magnification. Individual fibers were identified using the programs Adobe Photoshop and NIH ImageJ and the fiber area was calculated as a fraction of the total surface area.

The composite's void content was determined according to ASTM D792 [31] and ASTM D2734 [32]. Equation 2.5 is a method in [31] which determines the density of a panel by comparing its weight in air (mass dependent) to its weight when suspended in water by a wire (volume dependent). The measured density is compared to the theoretical density found with Equation 2.6. Differences between the theoretical density and measured density are assumed to be due to the presence of material voids, so Equation 2.7 is used calculate the void content.

$$D = \frac{a}{a + w - b}\rho_w \quad (2.5)$$

$$T = V_r \rho_r + V_m \rho_m \quad (2.6)$$

$$V_v = 100\frac{T - D}{T} \quad (2.7)$$

D -Measured density (kg/m^3)
T - Theoretical Density (kg/m^3)
a - Weight of dry specimen without wire (g)
b - Weight of wet specimen with wire (g)
w - Weight of wire (g)
ρ_w - Density of water (kg/m^3)
ρ_r - Density of reinforcement material (kg/m^3)
ρ_m - Density of matrix material (kg/m^3)
V_r - Volume fraction of reinforcement
V_m - Volume fraction of matrix
V_v - Volume fraction of voids

Scattering Control

The EWF method is subject to data scattering [24]. To produce quality data, specific efforts were made to ensure consistent tests.

Material voids introduced in the construction of the FRP panel reduce and randomize fracture toughness by acting as stress concentrations and extra crack nucleation points. The void content was reduced by using a vacuum chamber multiple times during the layup process. These vacuum stages removed air bubbles that were trapped during resin mixing and hand layup.

Concentrated loads applied by cutting tools can overstress thin crack tips and cause premature damage to test samples. Tool forces were minimized by using a low speed saw for cuts that could potentially damage crack tips.

Misalignment and friction cause mixed mode loading. Misaligned tabs contribute to data scatter by bending the sample when it is loaded in the Iosipescu fixture. Using positioner jigs ensured good, consistent alignment. Friction from the sliding jaws was prevented by using grease on the moving side.

Glue contaminating the cracks during tab bonding adds parasitic reinforcement. This was prevented by shielding the crack surface with tape.

Overstressing samples while loading them into the Iosipescu fixture would reduce their fracture toughness by causing premature damage. This was avoided by clamping the samples while the crosshead was moving, which allowed them to remain stationary, and unstressed.

Damaged samples were identified after data collection as the undamaged tests formed distinct data groupings, while damaged samples broke under a lower applied force. In early tests, the rejection rate of tests was 50%. The positioner jigs reduced the sample rejection rate to 10%.

Finite Element Model

A model of the DENS specimen was built using the commercial finite element program Abaqus 6.9. The objective of this model was to investigate the mechanisms of the behavior observed in the experiments.

Idealized Geometry

The microstructure has been idealized to a regular, symmetric pattern of fiber bundles. The spacing and bundle volume fraction are chosen such that the middle layers retain the average volume fraction of the actual material. The fiber bundles are modeled as rounded rectangles to remove complex geometry. Fiber bundles and the matrix resin are considered to be homogeneous materials, thus bundles are assumed to form fiber rich regions with resin rich regions between them. Figure 2.4 shows the idealized geometry for the middle layers, seen from the 2-3 material plane.

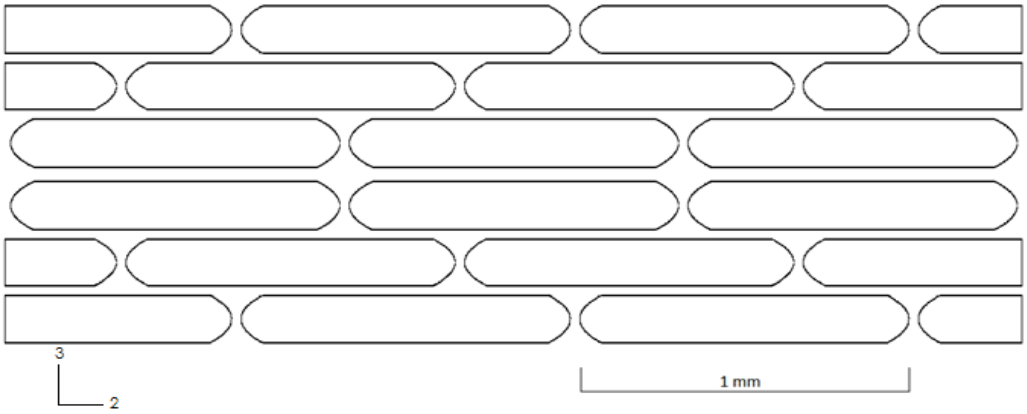

Figure 2.4: Idealized Geometry

FEM Construction

Since even the reduced geometry is complex, further simplification is needed to solve a model. The finite element model consists of a series of sections (1-3 plane) taken along the width of the specimen. Each section is a 2D plane strain model which allows the 3D behavior to be estimated under the assumption of a plane stain dominated system. A section model contains either three fiber bundles or two fiber bundles and a resin gap. A resin gap can occur in each of the three layers, on either side of the center, with symmetry preserved. The model of the test specimen in the Iosipescu fixture is shown in Figure 2.5. The fixture was modeled to capture any compliance due to the aluminum tabs.

The model of the specimen is shown in

Figure 2.6. The microstructure has been modeled in the middle with the outside edges modeled as uniform. At the center of the specimen, the individual fiber bundles are separated by resin rich regions. The fracture process zone has been represented using cohesive elements. Modeling the microstructure only in the middle is computationally efficient because the effects of shear damage are assumed to be localized.

The outer layers are homogeneous, orthotropic with the properties listed in Table 1. The elastic properties for the outside layers were estimated using Equations 2.8-2.12. These mixing rules were used assuming an average volume fraction of 25.4%.

$$E_1 = V_r E_r + V_m E_m \qquad (2.8)$$

$$\upsilon_{13} = V_r \upsilon_r + V_m \upsilon_m \qquad (2.9)$$

$$\frac{1}{E_2} = \frac{V_r}{E_r} + \frac{V_m}{E_m} \qquad (2.10)$$

$$\frac{1.38}{E_3} = \frac{V_r}{E_r} + \frac{V_m}{E_m} \qquad (2.11)$$

$$\frac{1}{G_{13}} = \frac{V_r}{G_r} + \frac{V_m}{G_m} \qquad (2.12)$$

E_1 - Elastic modulus in the fiber direction (MPa)
E_2 - Elastic modulus for the in plane direction (MPa)
E_3 - Elastic modulus for the transverse direction (MPa)
ν_{13} - Poisson's ratio for the out of plane direction
G_{13} - Shear modulus for the out of plane direction (MPa)

At the center of the specimen, the individual fiber bundles are separated by resin rich, interlaminar regions. Lamina properties for 45% [33] were assumed to represent the elastic response of the fiber bundles. The plastic response of the fiber bundles is governed by the Hill plasticity model [34]. The resin rich regions are isotropic with elastic-plastic properties based on the work of Hu, Xia, and Ellyin [28], who tested the epoxy used in the present work. Resin rich regions are represented as a stiffened epoxy, since they still contain some reinforcement fiber. Figure 2.7 shows the original and modified elastic-plastic response of the resin rich regions. The stiffness of resin rich regions was scaled to support the empirical fracture stress.

Cohesive elements form the fracture process zone in the center of the DENS specimen. The cohesive zone is one element thick and transfers stress from one side to the other as a surface traction. Damage is modeled in this area as a degrading stiffness and eventual separation.

The glue bonding the specimen to the tabs is modeled with cohesive elements in order to take advantage of their surface traction formulation. Shear traction stiffness of the adhesive surface was set at 150 MPa/mm. The glue is assumed to be rigid under normal loading so its normal stiffness was set to be 10^7 MPa/mm. The tab-specimen interface does not model damage (i.e. it can stretch but not slip).

The aluminum tabs and steel jaws were sized and positioned to be the same as in the experiment. Contact is defined between the tabs and jaws to provide realistic clamping, with the coefficient of static friction set at 0.47 [35]. Boundary conditions are enforced at the outside edges of the moving and fixed Iosipescu jaws, which are rigid surfaces.

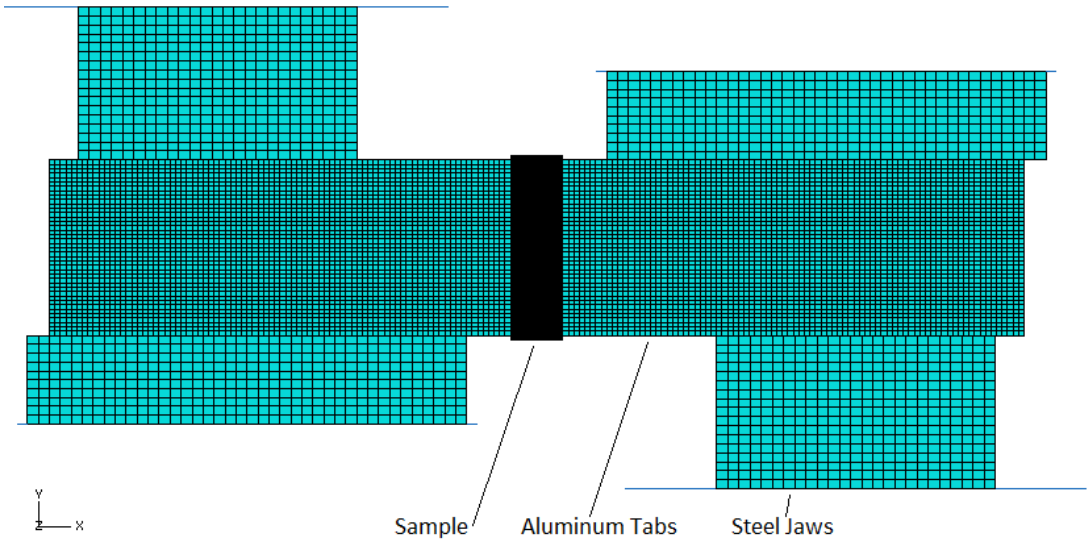

Figure 2.5: Finite Element Model of the Iosipescu DENS Test

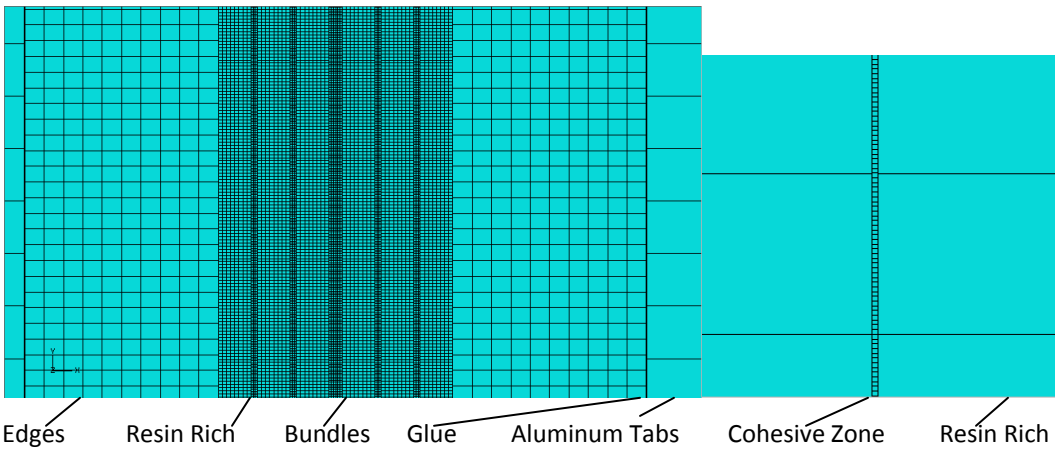

Figure 2.6: Model of the DENS specimen

Table 2.1: Elastic Properties

Material	E_1	E_2	E_3	ν_{12}	ν_{13}	ν_{23}	G_{12}	G_{13}	G_{23}
Outer Layer	24100	6200	4500	0.275	0.275	0.3	1800	1800	1300
Fiber Bundle	38600	8270	8270	0.26	0.26	0.321	4140	4140	3130
Resin Rich	3872	-	-	-	0.42	-	-	-	-
Aluminum Tab	70000	-	-	-	0.33	-	-	-	-
Steel Jaw	200000	-	-	-	0.30	-	-	-	-

Stress reported in MPa

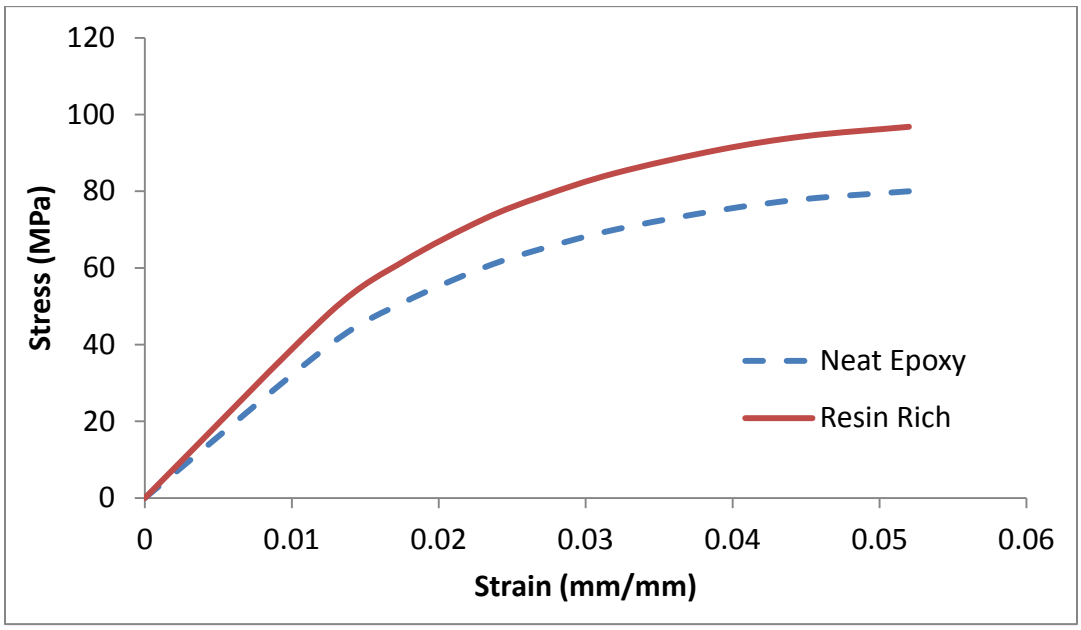

Figure 2.7: Resin Rich Response

Hill Plasticity Model

The fiber bundles require an initiation criterion and evolution law that considers orthotropic behavior. For an orthotropic material, the simple von Mises plasticity model is inadequate. Hill's yield criterion is an adaptation of the von Mises which assigns a relative weight to each stress component to define an equivalent stress. Equation 2.13 is the Hill stress function. The Hill potentials are determined using yield ratios, defined as the ratio of the yield stress under a unidirectional stress state, relative to a reference yield stress [36]. The reference yield stress used here is the yield stress of epoxy.

$$f(\sigma)=\sqrt{F(\sigma_{22}-\sigma_{33})^2+G(\sigma_{33}-\sigma_{11})^2+H(\sigma_{11}-\sigma_{22})^2+2L\sigma_{23}^2+2M\sigma_{31}^2+2N\sigma_{12}^2}$$

$$\begin{aligned} F&=\frac{1}{2}\left(\frac{1}{R_{22}^2}+\frac{1}{R_{33}^2}-\frac{1}{R_{11}^2}\right), & L&=\frac{3}{2R_{23}^2},\\ G&=\frac{1}{2}\left(\frac{1}{R_{33}^2}+\frac{1}{R_{11}^2}-\frac{1}{R_{22}^2}\right), & M&=\frac{3}{2R_{13}^2}, \quad R_{ij}=\frac{\bar{\sigma}_{ij}}{\sigma^0}\\ H&=\frac{1}{2}\left(\frac{1}{R_{11}^2}+\frac{1}{R_{22}^2}-\frac{1}{R_{33}^2}\right), & N&=\frac{3}{2R_{12}^2}, \end{aligned} \qquad (2.13)$$

The Hill potentials were set such that the yield criterion only responds to transverse normal stress (in direction 2 or 3) and shear. The yield ratios and their corresponding Hill potentials are listed in Table 2. The reference yield stress for the fiber bundles is the plastic response of neat epoxy. The bundles can therefore be deformed in a manner similar to epoxy under transverse tension and shear, but remain elastic in the fiber direction. The stress response for this epoxy was demonstrated to be independent of hydrostatic pressure [28], thus the Hill stress response can be based on the von Mises stress response, since they are both derived from distortion energy.

Table 2.2: Hill Coefficients

Yield Ratio	**R_1**	**R_2**	**R_3**	**R_{12}**	**R_{13}**	**R_{23}**
	100	1	1	1	1	100
Hill Potential	**F**	**G**	**H**	**L**	**M**	**N**
	0.99995	0.00005	0.00005	0.00015	1.5	1.5

Cohesive Elements

Cohesive elements are interface elements which represent a potential crack surface. The behavior of these elements is based on the cohesive zone model [37, 38]. This model assumes that cohesion is maintained by a surface traction during damage, which allows the modeling of progressive failure.

Interface stiffness in a cohesive element is expressed as a stress (normal or shear) per relative separation of the crack surfaces. This is known as a traction-separation stiffness model. The local element coordinate system remains fixed, which maintains the surface normal and tangent directions under large deformation.

Damage is modeled by degrading the element's stiffness and tracked using a scalar damage variable. Representing damage by a stiffness reduction is called an elastic damage model. The damage variable for an element is between 0 (undamaged) and 1 (completely damaged). Damage is initiated when a stress component (in this case shear stress) reaches its maximum value. Further separation results in damage propagation. Damage propagation is governed by Equation 2.14 and the corresponding stiffness is governed by Equation 2.15. The resulting softening behavior for a cohesive element is demonstrated in Figure 2.8.

$$D = \frac{\delta_f(\delta_{\max} - \delta_0)}{\delta_{\max}(\delta_f - \delta_0)}, \quad \delta_f = \frac{2G}{\tau_{\text{int}}}, \quad \delta_0 = \frac{\tau_{\text{int}}}{K_0} \qquad (2.14)$$

$$K = (1 - D)K_0 \qquad (2.15)$$

D – Damage coefficient
K – Degraded stiffness (MPa/mm)
K_0 – Undamaged element stiffness (MPa/mm)
δ_{max} – Maximum displacement in load history (mm)
δ_f – Fracture displacement (mm)
δ_0 – Displacement at damage initiation (mm)
τ_{int} – Damage initiation stress (MPa)

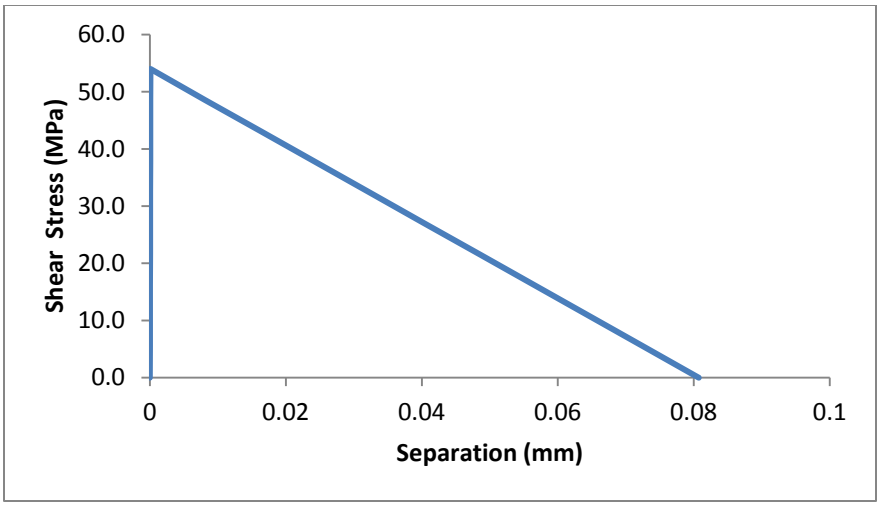

Figure 2.8: Softening of Cohesive Elements

The initial stiffness of the cohesive zone was determined by adapting a technique proposed by Turon et al. for mode I delamination in a double cantilevered beam specimen [39]. Equation 2.16 is the stiffness equation used in [39]. Turon used the half-laminate thickness as the characteristic thickness and recommended a scale parameter (α) between 50 and 100. Equation 2.17 is the adapted form for mode II stiffness.

$$K_{nn} = \frac{\alpha E_{33}}{t} \qquad (2.16)$$

$$K_{ss} = \frac{\alpha G_{13}}{t} \qquad (2.17)$$

K_{nn} – Stiffness in normal direction (MPa/mm)
K_{ss} – Stiffness in tangent direction (MPa/mm)
E_{33} – Transverse elastic modulus (MPa)
G_{13} – Out of plane shear modulus (MPa)
t – Characteristic length (mm)
α - Scaling parameter

The cohesive zone must be stiff enough to prevent extra compliance from being introduced to the system [39]. The characteristic length used in the present work was the thickness of the resin rich region between bundles. A scaling value of 50 was used for α, which gives interface stiffness values of $K_{nn}=2.07\text{x}10^{7}$ and $K_{ss}=7.22\text{x}10^{5}$ MPa/mm. Based on observations from the conducted experiments, the maximum shear stress was set to 54 MPa and the EWF was set to 2.18 kJ/m^2.

The Riks Arc Length Method

The final step of the simulation is a method proposed by Riks [40], and adapted for finite element solvers by Crisfield [41]. This method was designed to model the behavior of unstable systems by simultaneously solving for force and displacement.

The Riks method tracks a solution by arc length, which is a non physical parameter to measure the "length" of a solution curve in a multidimensional solution space. The arc length increment is defined by Equation 2.18 [41]. Equation 2.18 places an additional requirement on the force and displacement parameters so they may be considered a single degree of freedom. The arc length constraint is evaluated in addition to Equation 2.19, which is the global stiffness equation.

The load vector is controlled by a reference load and a load proportionality factor. The load proportionality factor provides a dimensionless scalar with which to track the solution. Solutions are incremented by arc length, then an equilibrium position, that fits the required arc length, is determined using the Newton-Raphson procedure. The process is illustrated in Figure 2.9.

$$\Delta u^T \Delta u + \Delta\lambda^2 p^T p = \Delta l^2 \quad (2.18)$$

$$Ku = f \quad (2.19)$$

u - displacement vector
p - reference load vector
f - nodal load vector
K- stiffness matrix
λ - load proportionality factor
l - arc length

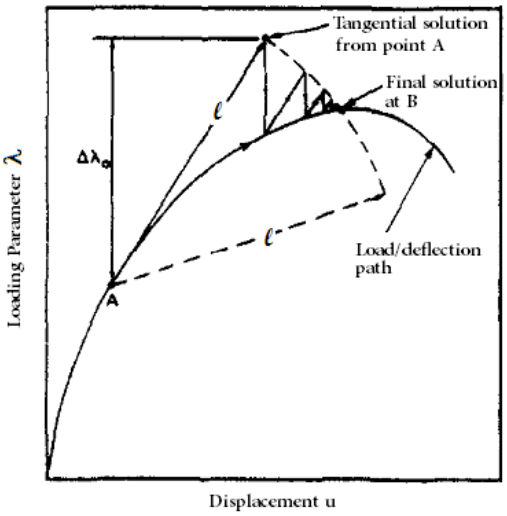

Figure 2.9: The Riks Method [41]

Virtual Experiment in FEM

The first step in the virtual experiment is to clamp the tabs into the simulated Iosipescu fixture. A force of 10 N/mm is applied to the two movable jaws while the other two jaws are held fixed. The clamping force was chosen to be large enough to prevent the tabs from slipping out of the jaws. This is considered the starting position for the virtual experiment.

During the loading step, the fixed side is constrained in both directions. The displacement on the moving side is applied in the vertical direction only, with its horizontal position fixed (a roller condition). This single degree of freedom is due to the boundary condition being applied on the edge of the Iosipescu jaws, thus the aluminum tab surfaces are still permitted to deform in both directions. The applied force is the sum of reaction forces from the jaws' rigid surfaces, representing the net external force applied by the crosshead. Displacement stroke is measured from the top of the fixed jaw, on the moving side.

After reaching its maximum load, the displacement controlled step ends and is replaced with a Riks arc length step. Simulation continues under arc length control until the two halves of the model are completely separated.

FEM Validation with Uncracked Specimen

An uncracked specimen was used to validate the choice of material properties in the finite element model. The uncracked DENS specimen has the same dimensions but did not have a starter film, so it represents undamaged material. To test the uncracked specimen for nonlinearity and plasticity, it was loaded and unloaded to 1200 N, 2400 N, then 3600 N. A total of 5 uncracked samples were tested.

To represent the uncracked specimen in the model, the ligament area was removed and the two sides were connected directly. Therefore, damage is not modeled, but plasticity still is. The stiffness in the virtual experiment is compared to the stiffness in the physical experiment to assess the accuracy of the model.

Chapter 3 - Results

Introduction

The results of experiments and finite element simulations are presented in this chapter. The material microstructure is characterized and quantified. The measured fracture energy from experiments is presented and the functional mechanism of the Iosipescu DENS test is determined using a finite element model. The model is then validated against experiment data from two different types of Iosipescu specimens.

Material Characterization

The microstructure of a DENS sample is shown in Figure 3.1. This is the ligament area of an unbroken sample, cut through the 2-3 material plane. The average fiber volume fraction is 29.2%, but it is not uniformly distributed. The outer layers are sparse, and individual fiber bundles are clearly visible. These outside areas have an average fiber volume fraction of 25.4% while individual bundles are between 45% and 60%. Since the stitching threads were removed in the middle layers, the fiber bundles have spread out more than at the edges. This caused a near uniform distribution of the glass fibers with an average volume fraction of 38.6%, although individual fiber bundles are visible due to resin rich regions between them. The boundary between the outer and middle layers is distinct, allowing the middle's average thickness to be measured as 39.5% of the total surface. The dark spots in Figure 3.1 are material voids.

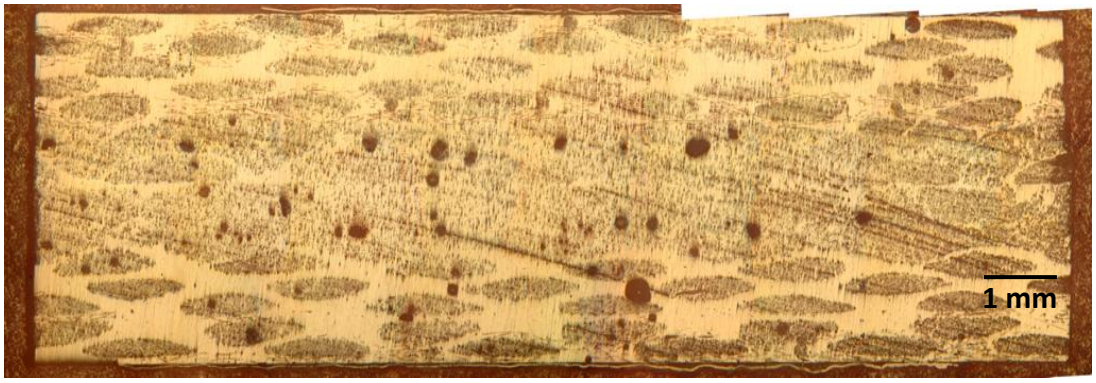

Figure 3.1: Microstructure of the DENS Specimen

In addition to microscopy, the fiber volume fraction was calculated according to Equation 2.3 using layer thickness values h_a=0.605h, and h_b=0.395h. When calculated from Equation 2.3, the volume fractions of the outer and middle layers are 21% and 38% respectively.

Three pieces of the composite panels were tested according to ASTM D2734 to determine the material's void content. The pieces had an average void content of 2.5% and an average material density of 1584 kg/m^3. The properties for all the inspected samples are summarized in Table 3.1.

Table 3.1: Properties of Inspected Samples

Source	Average V_f	void content	density (kg/m^3)	outer V_f	middle V_f
Microscopy	29.2%	-	-	25.4%	38.6%
Panel Sample 1	27.5%	2.8%	1578	20.7%	37.9%
Panel Sample 2	27.8%	1.5%	1593	20.9%	38.3%
Panel Sample 3	28.6%	3.1%	1580	21.5%	39.4%
Panel Averages	29.2%	2.5%	1584	21.0%	38.5%

Iosipescu DENS Results

A typical result of an Iosipescu DENS test is shown in Figure 3.2. The test consists of: 1) a short takeoff distance in which the fixture is settling, 2) a linear region under stable loading, 3) a short softening region, 4) a sudden, unstable crack growth. Fracture displacement is measured at the peak load, because it is the most reliably identified point on each test curve.

The specific work of fracture (SWF) for all ligament lengths is given in Figure 3.3. Takeoff distances were removed from the SWF calculation by extrapolating their linear region back to zero load. The SWF trend initially follows the linear increase with ligament area that is required for the essential work of fracture (EWF) method. Extrapolating a linear best fit line from data for ligament lengths in the range of 2 to 5 mm gives an EWF of 2.18 kJ/m^2.

Data for the 6mm ligament length deviates from the linear trend by forming a SWF plateau. For this ligament length, the deformation is driven by fiber buckling. The evidence for a change in deformation mechanism is found on the fracture surfaces. Figure 3.4 shows the fracture surface of a 5 mm sample and a 6 mm sample. The 5 mm sample has a clear, sharp edge dividing the fracture surface from the rest of the sample's area. A sharp edge is typical of all ligament lengths except for the 6 mm. For the 6 mm, pulled out fibers cross the boundary between the fracture surface and the rest of the sample, which suggests mode I loading is present. Evidence for fiber draping is seen in Figure 3.5, which was taken from the ligament area of a 6 mm sample in the 1-3 material plane. Fibers in the fracture process zone are seen to bend into the crack growth path, which makes them more susceptible to buckling than the shorter lengths. Furthermore, Table 3.2 shows the 6 mm samples had a lower initial stiffness than the 5 mm. Figure 3.6 shows the breaking force did not increase, between the 5 and 6 mm samples. The fracture displacement did however increase, as seen in Figure 3.7.

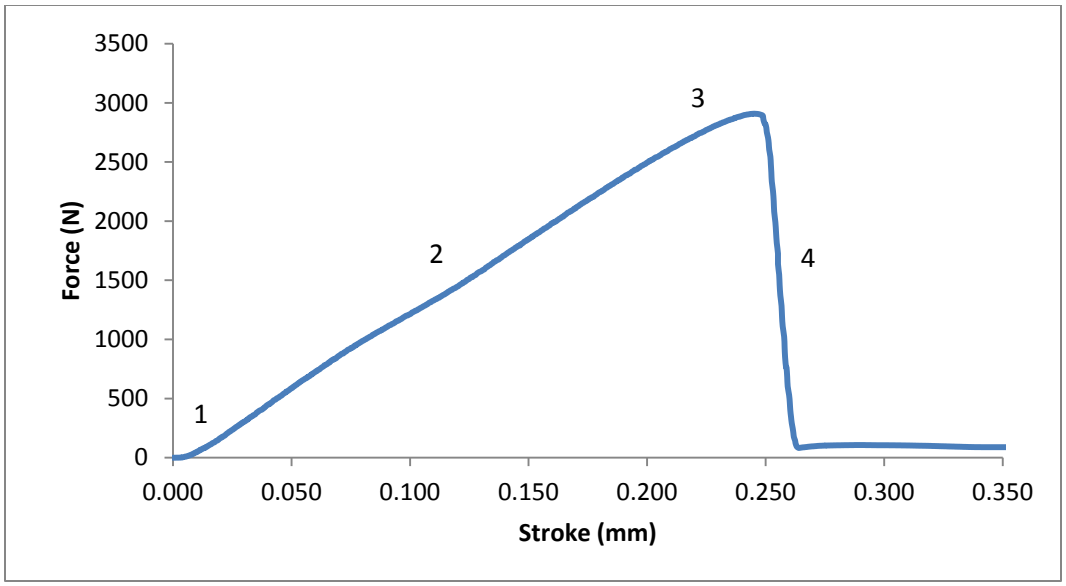

Figure 3.2: A Typical Iosipescu DENS test

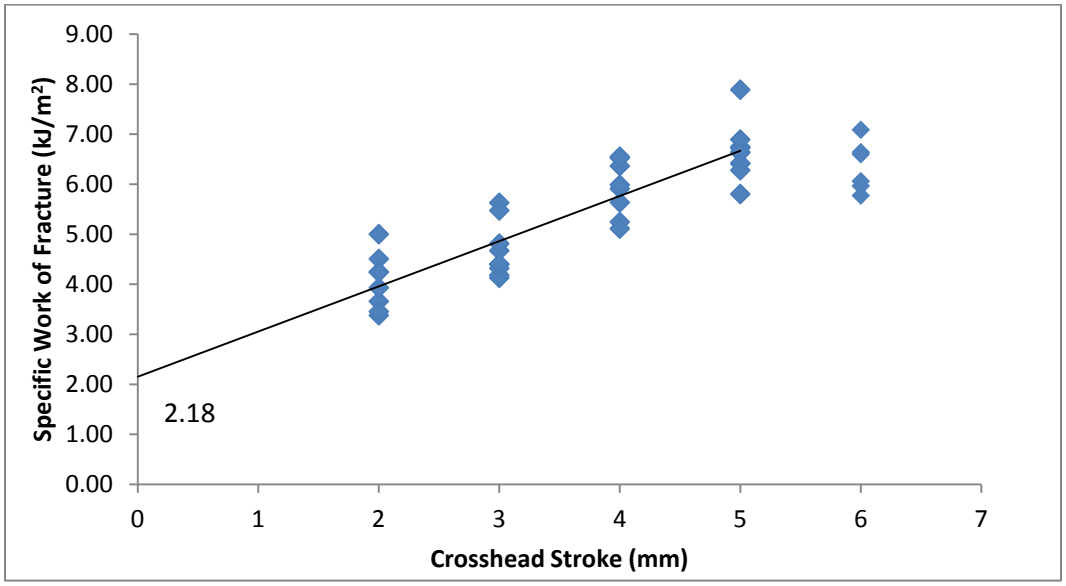

Figure 3.3: Specific Work of Fracture in all Ligament Lengths

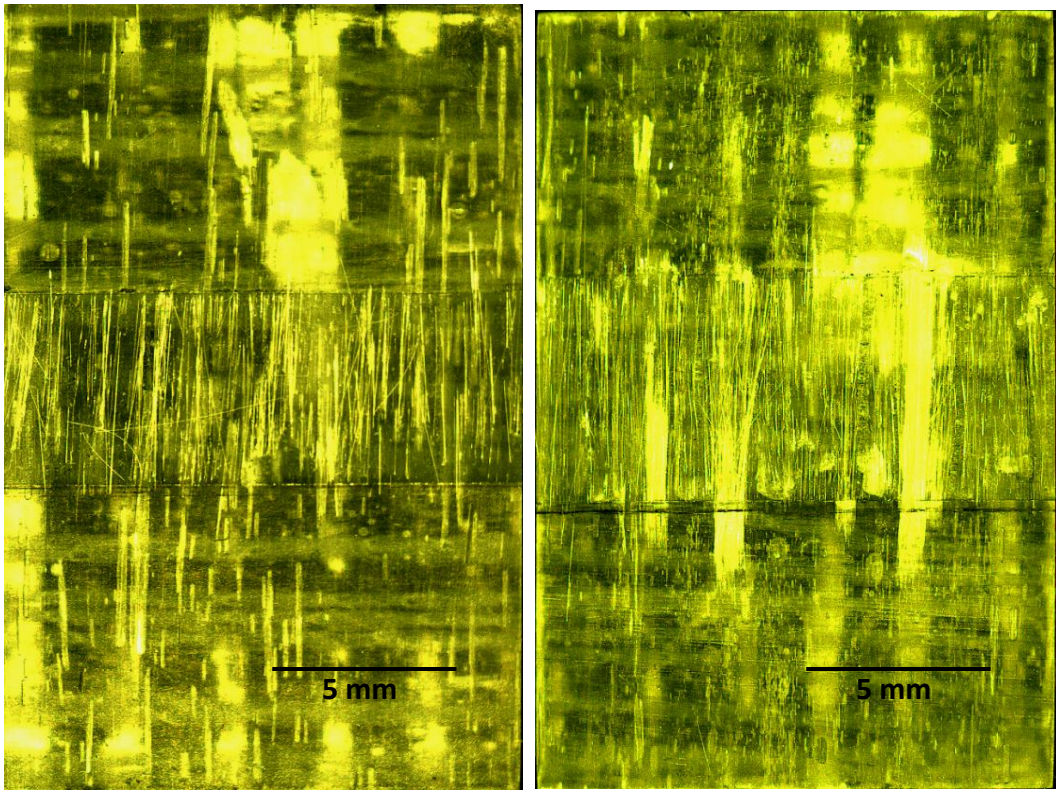

Figure 3.4: Iosipescu Fracture Surfaces: 5mm ligament (left) and 6mm ligament (right)

Figure 3.5: Fibers in the Ligament Area

Table 3.2: Stiffness of the DENS Samples

Ligament Length (mm)	**2**	**3**	**4**	**5**	**6**
Average Stiffness (N/mm^2)	769	882	933	998	890

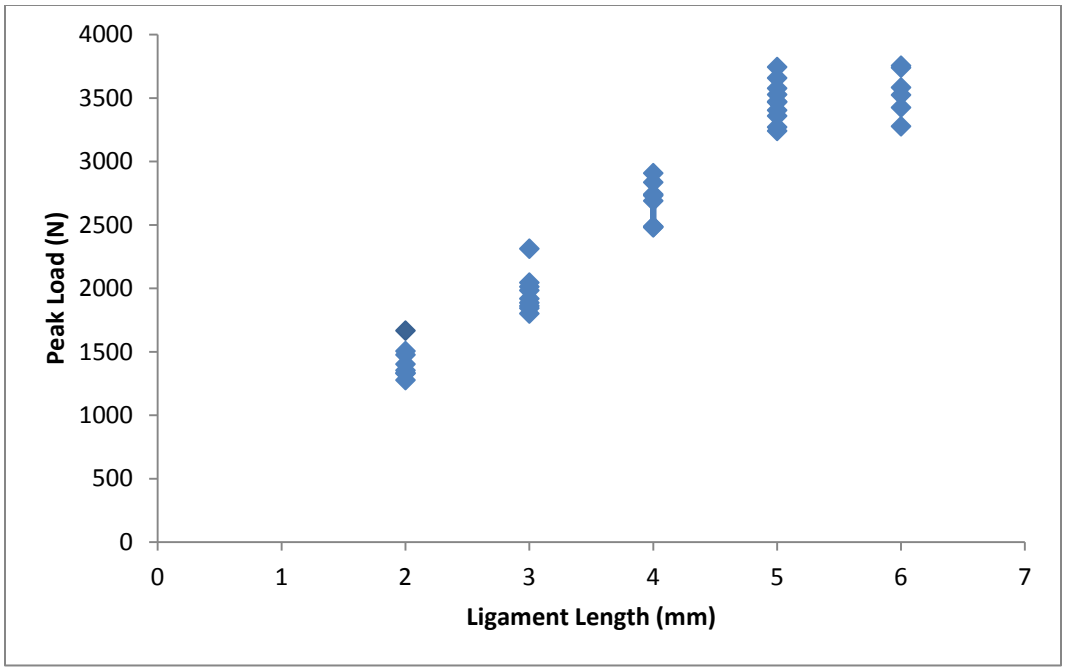

Figure 3.6: Peak Load of Iosipescu DENS Test

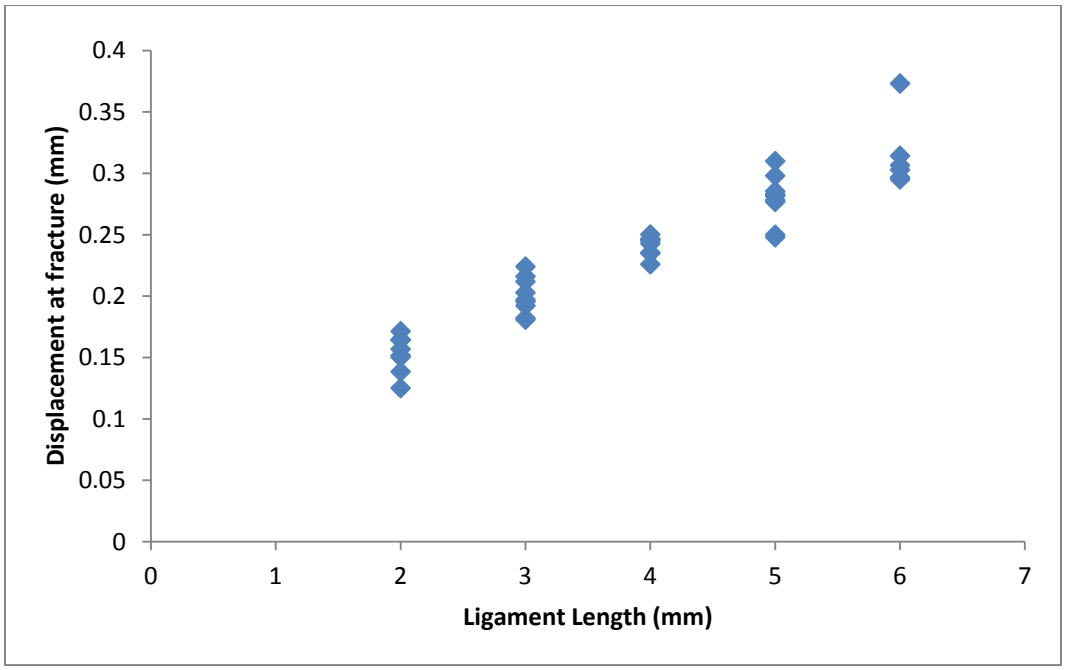

Figure 3.7: Fracture Displacement of Iosipescu DENS Test

Consistency in sample thickness was difficult to obtain, but all test results were independent of thickness, within the range used for the experiments. Figure 3.8 shows the peak load and Figure 3.9 shows the fracture displacement, each plotted against the sample thickness. Neither the peak load nor the fracture displacement shows any significant change within the range of 4.2 – 4.8 mm.

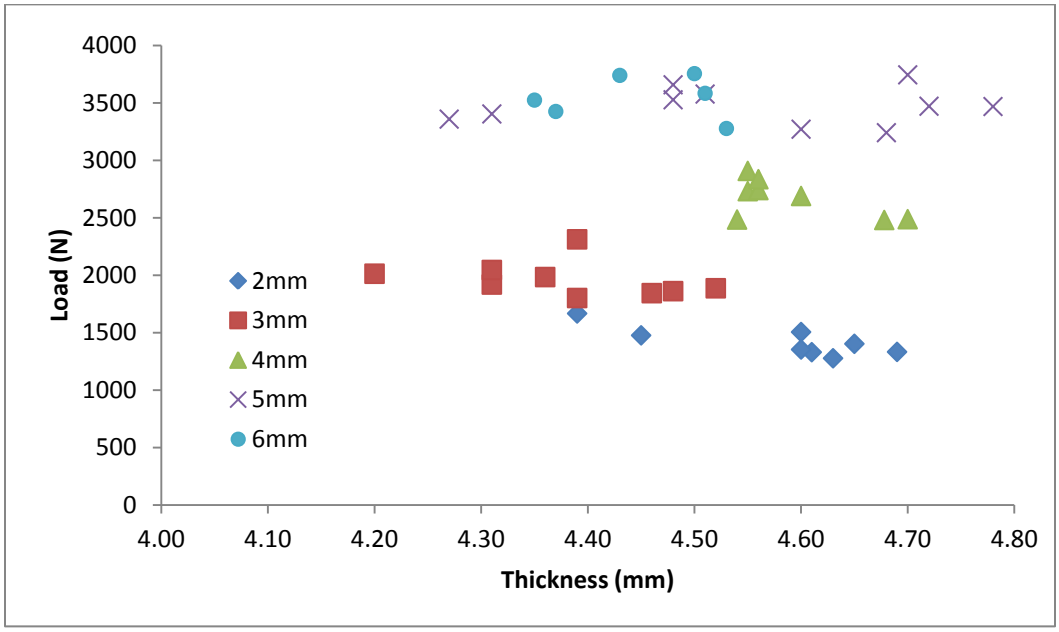

Figure 3.8: Thickness Independence of Peak Loads

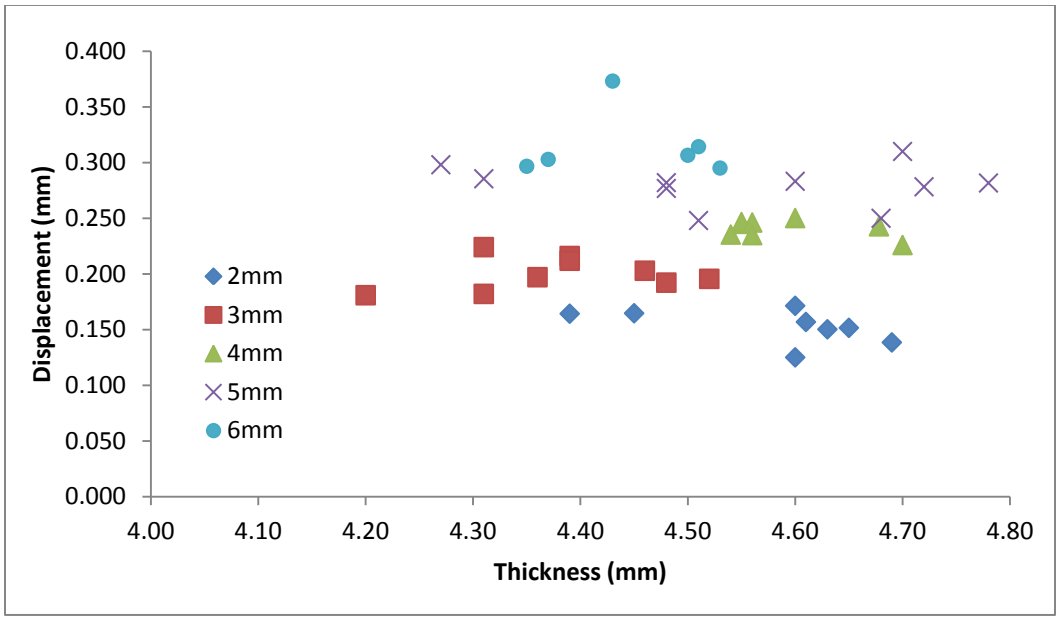

Figure 3.9: Thickness Independence of Fracture Displacements

Self similarity between the load curves is a way of confirming that all the sample sizes are deforming under the same mechanism. In Figure 3.10, the force has been normalized by the maximum load and the displacement has been normalized by the fracture displacement. When normalized, representative curves from each ligament length are plotted together they are seen to be self similar.

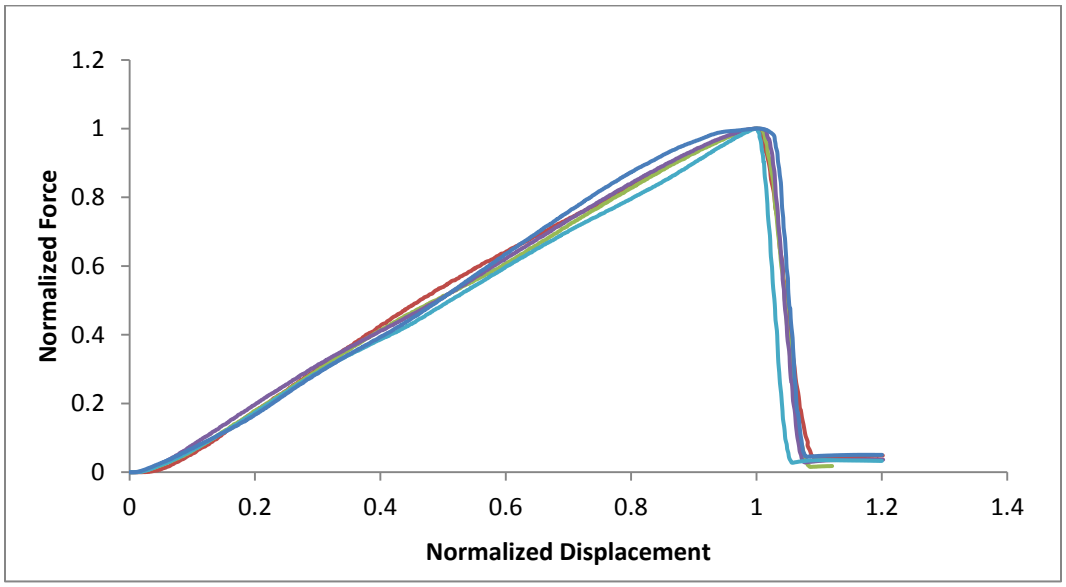

Figure 3.10: Normalized Results from the IDENS Test

ENF Results

Six ENF samples were tested and a typical result shown in Figure 3.11. The test curve consists of: 1) a linear response region, 2) a short softening region, 3) a sudden load drop due to unstable crack growth. The critical energy release (G_{IIc}) rate is calculated from Equation 2.1 using three load values from the ESIS Protocol [29]. Using the non-linear point, G_{IIc} is 2.35 kJ/m^2. Using the 5% offset load, G_{IIc} is 3.39 kJ/m^2. Using the maximum load, G_{IIc} is 3.44 kJ/m^2. The standard deviation of non-linear, offset, and maximum load values are 0.29, 0.30, and 0.34 kJ/m^2 respectively.

The fracture energy from the ENF test is compared with the IDENS data in Figure 3.12. The data scatter from the Iosipescu DENS test predicts an EWF between 1.5 and 3.1 kJ/m^2, which is in agreement with the G_{IIc} value calculated from the non linear point of the ENF test. The other two loads give a higher fracture energy than the IDENS.

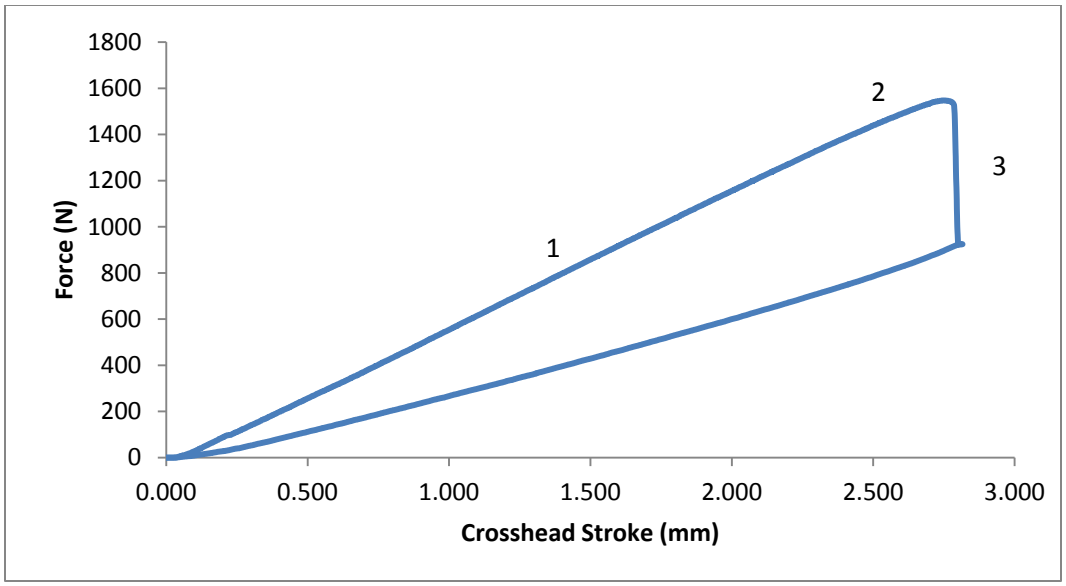

Figure 3.11: A Typical ENF Test

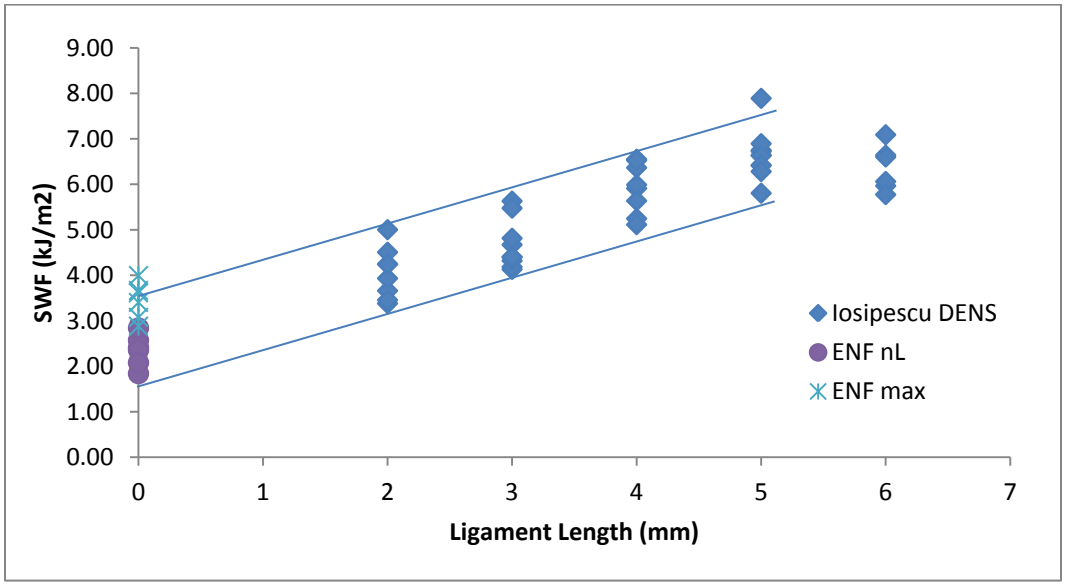

Figure 3.12: Iosipescu DENS Compared to ENF

Model Validation

Although four cross sections are required to represent the 3D response of the DENS specimen, its response is accurately represented by the three bundle version. Table 3.3 shows that since the gap sections are so much thinner than the bundle sections, they don't contribute to the stiffness of the specimen. By approximating the entire specimen as a three bundle section, the overall stiffness is increased by less than 1%.

Using the three bundle approximation, the finite element model was able to reproduce the behavior of the experiments. The maximum force, average stress, and breaking displacement are within the scatter of experiment data. The model results are compared with the experiment results in Figure 3.13, Figure 3.14, and Figure 3.15. There is no FEM data for the 6 mm ligament length because the model does not consider fiber buckling, and therefore does not hold for this length.

Table 3.3: Stiffness of Model Sections

Section	Total Thickness (mm)	Stiffness (N/mm)	Relative to Bundles (%)
3 Bundles	11.999	11147	100%
Gap 1	0.667	577	5.2%
Gap 2	0.667	602	5.4%
Gap 3	0.667	607	5.4%

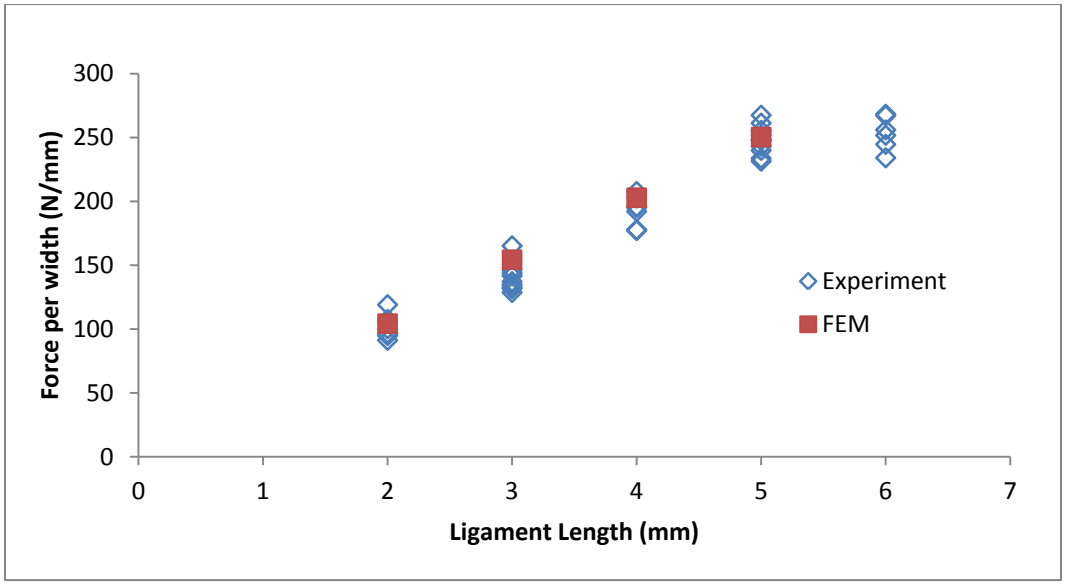

Figure 3.13: Maximum Force in FE Model

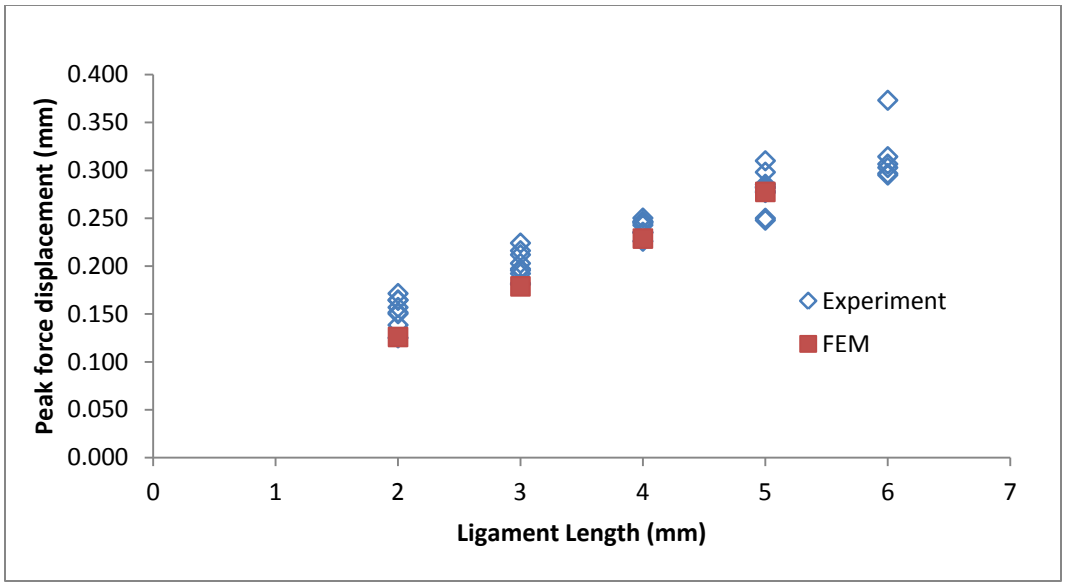

Figure 3.14: Breaking Displacement in FEM

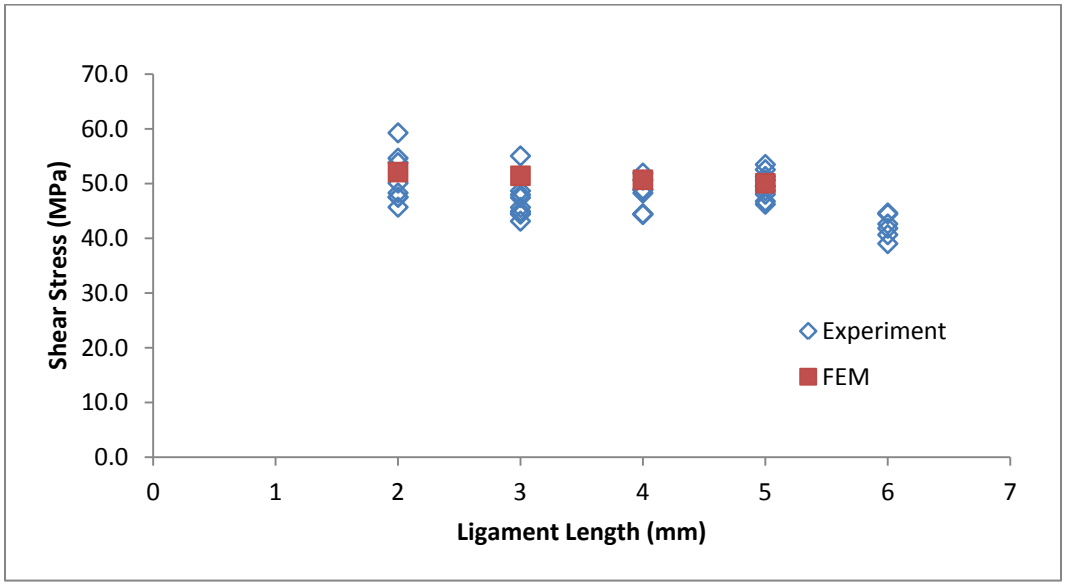

Figure 3.15: Maximum Nominal Stress in FEM

Figure 3.16 shows a typical test of an uncracked specimen. The uncracked samples have a longer takeoff, which makes their initial behavior (below 500 N) difficult to determine. The uncracked specimen has a nonlinear load curve and an initial hysteresis loop. The hysteresis loop is caused by the friction between the tabs and fixture. Upon unloading, the hysteresis loop eventually converges to the loading curve, which shows that the uncracked specimen is elastic. Above loads of 500 N, a linear regression is a good curve fit (correlation coefficient R^2=0.99) if applied to the loading phase while ignoring the unloading phase. Using this fitted curve, the average linear stiffness of the uncracked samples was

14850 N/mm. The initial slope of a simulated uncracked sample was 14155 N/mm, which is only 5% stiffer than in the experiment.

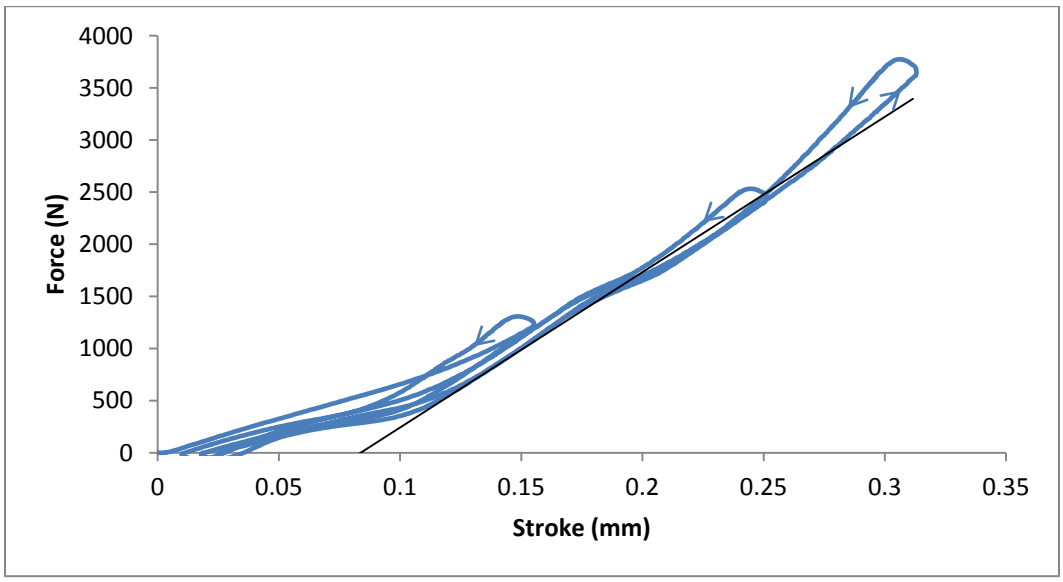

Figure 3.16: Test of Uncracked Specimen

Finite Element Results

The simulation results for ligament lengths 2-5 mm are shown in Figure 3.17. Before their peak load, all sizes show the same initial behavior as the experiments: there is a long, linear section then a small softening. After the peak load, damage propagates with the displacement direction reversed, rather than at constant displacement. This reverse in direction takes place under the Riks phase of the solution and represents the path of stable crack growth. If it were possible to configure a test to unload a specimen along this path, stable crack growth would be generated. If SWF is determined using the applied work at the peak load, it is 0.95 kJ/m^2. If the unloading due to complete fracture is considered, then the EWF is 2.24 kJ/m^2, which is close to the given material property of 2.18 kJ/m^2. Figure 3.18 demonstrates that the trend of SWF values has a shallower slope if the unstable fracture is completed in a stable manner.

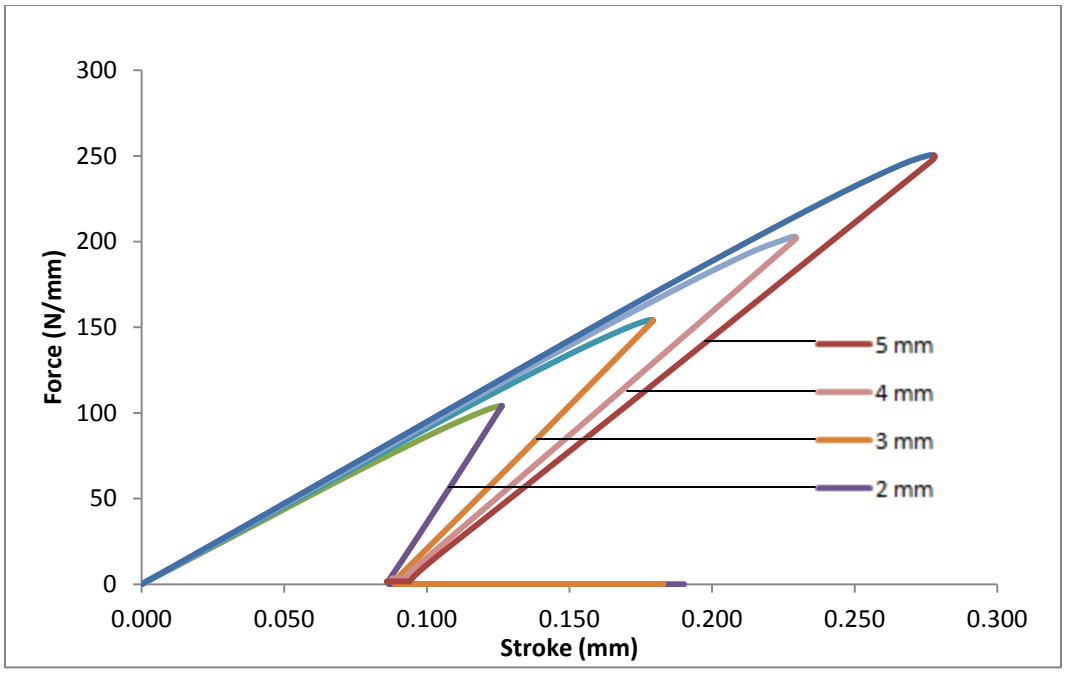

Figure 3.17: Virtual Experiment

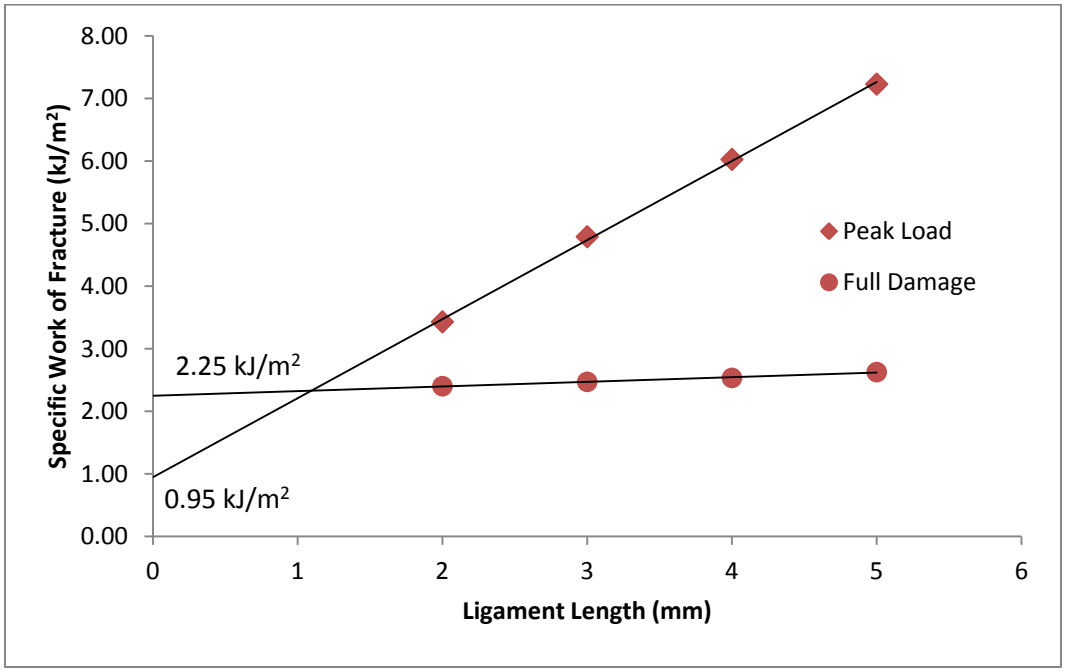

Figure 3.18: EWF of Virtual Iosipescu DENS

When the EWF method is applied to ductile materials such as metals and polymers, the linear increase of SWF is due to an increase in plastic deformation energy. This is not the case with the composite material studied here. External work is stored mainly as strain energy, with little plastic deformation. Table 3.4 shows the relative energy content of the DENS specimen by ligament length.

The plastic deformation is localized to the interlaminar region, with only small propagation into the first layer of fiber bundles. Thus, the fiber layers are creating a barrier that limits damage, as demonstrated in Figure 3.19. Conversely, the strain energy forms an elliptical distribution around the ligament area which is shown in Figure 3.20. Since the strain energy is penetrating from the ligament area into the bulk material, it has a linear dependence on ligament area and is analogous to the plastic energy in ductile materials. If the stable unloading path could be generated, all strain energy would be released and the linear change of SWF would be driven by plastic energy, which is seen in Figure 3.18 to have a much smaller increase with ligament length.

Table 3.4: Relative Energy Content of DENS Specimen at Maximum Load

	2mm	**3mm**	**4mm**	**5mm**
Strain Energy	74.2%	73.8%	73.4%	71.8%
Plasticity Losses	19.6%	19.9%	20.2%	21.4%
Damage Energy	6.2%	6.3%	6.4%	6.7%

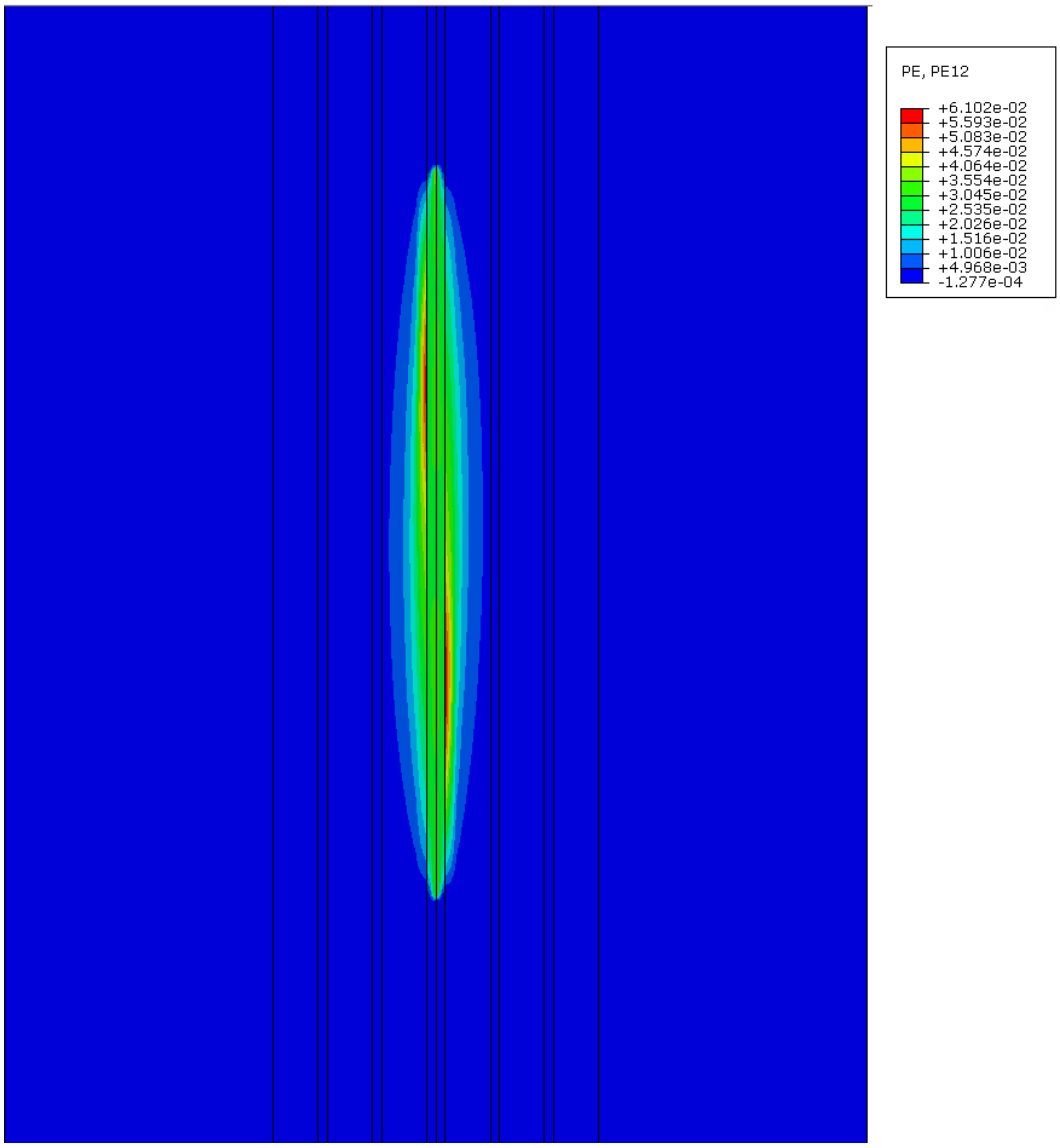

Figure 3.19: Plastic Shear Strain in 4mm

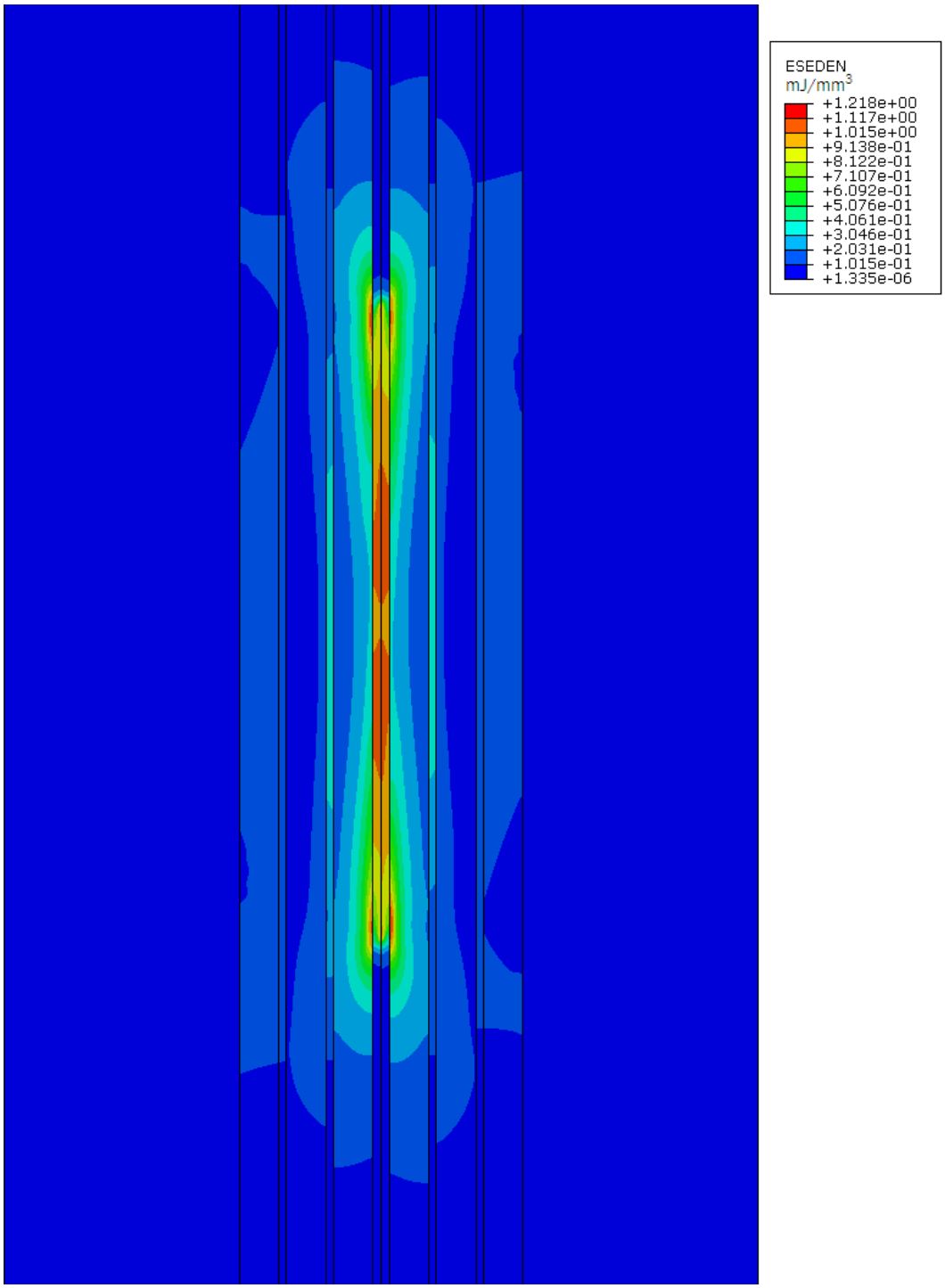

Figure 3.20: Strain Energy Density in 4mm

The distribution of contact pressure along the tabs is shown in Figure 3.21 for the 4mm ligament length, at maximum load. The load resembles that of a four point asymmetric beam, which demonstrates how the Iosipescu fixture creates shear loading.

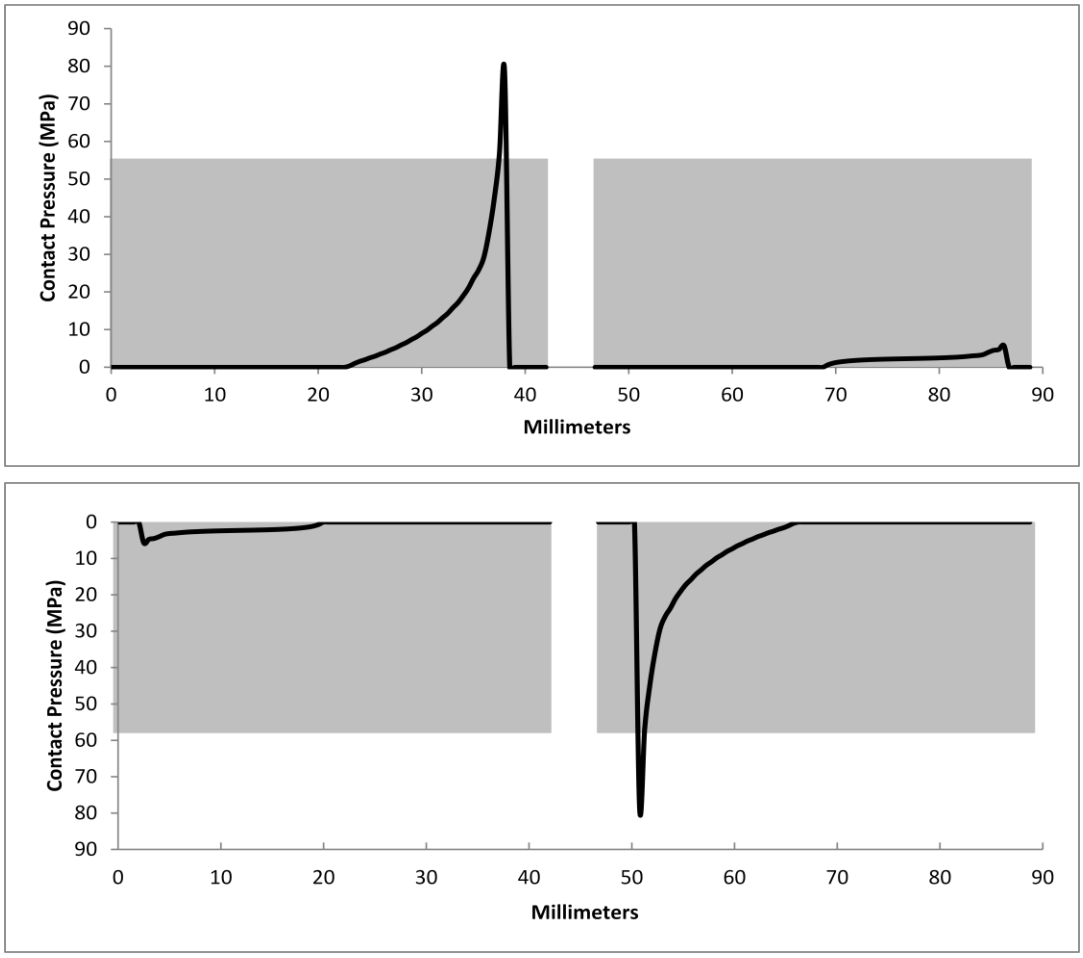

Figure 3.21: Contact Pressure From the Iosipescu Fixture

Interlaminar stress characteristics are demonstrated for the model of 5mm ligament length at the points identified in Figure 3.22. Points A, B, and C are the linear region in which damage effects are negligible. Points D, E, F are in a region of damage propagation. Point F is the peak load and Point G is the end of stable growth that occurs soon after the peak load.

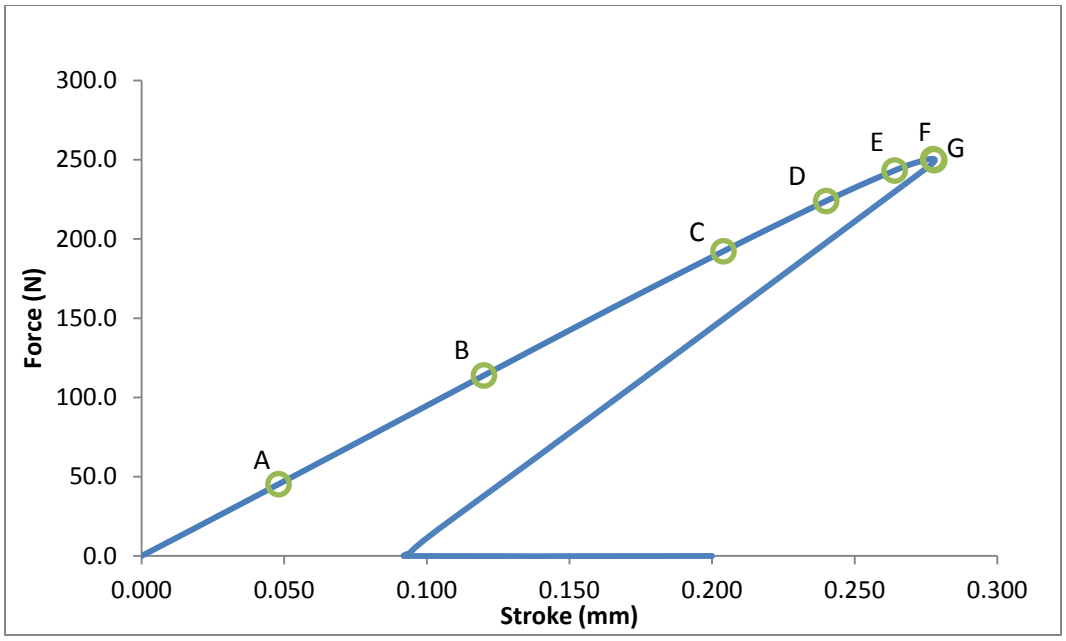

Figure 3.22: Virtual Test of the 5mm Iosipescu DENS

The simulated stress state along the ligament length is seen in Figure 3.23 to be non-uniform for all applied loads. Shear stress is concentrated at the crack tips due to the discontinuity there and reaches a maximum value when damage is initiated. Although the stress state is not uniform, it is shear dominated for all applied loads. The normal stress along the ligament length is compressive, finite, and always smaller than the shear stress. Ligament normal stress is plotted in Figure 3.24. At the crack tips, there are high compressive stress due to the discontinuity and finite ligament thickness. This effect is extremely localized, so it does not significantly contribute to bulk effects and normal stress is ignored by the damage model.

Element damage coefficients are plotted along the ligament length in Figure 3.25 for the load levels in Figure 3.22. The initial propagation is slow and driven by the stress singularity at the crack tips. Although this initial damage propagation is artificial (a result of FEA) it is mitigated by the cohesive zone model. The ligament area is not fully damaged at the peak load or even the stability limit. After reaching a critical damage threshold, further damage results in a stress distribution that is unable to balance the applied load, causing further crack growth which releases strain energy from the surrounding areas. This energy release creates unstable crack growth if the EWF is too low. Figure 3.26 shows a transition to stable crack growth if the EWF exceeds 6 kJ/m^2.

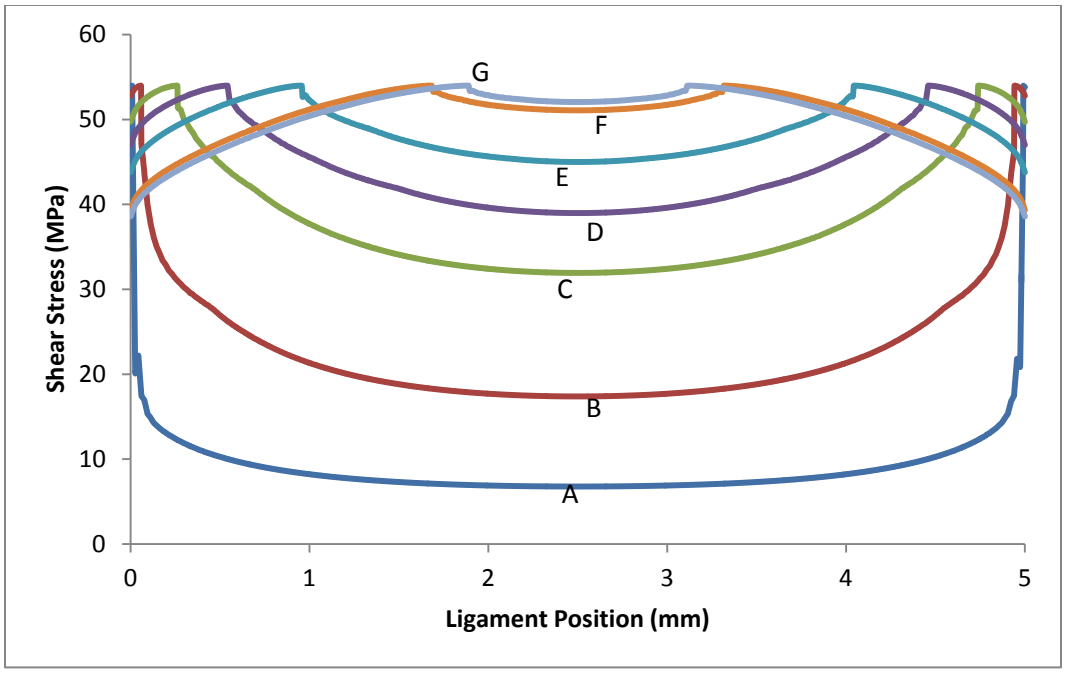

Figure 3.23: Ligament Shear Stress

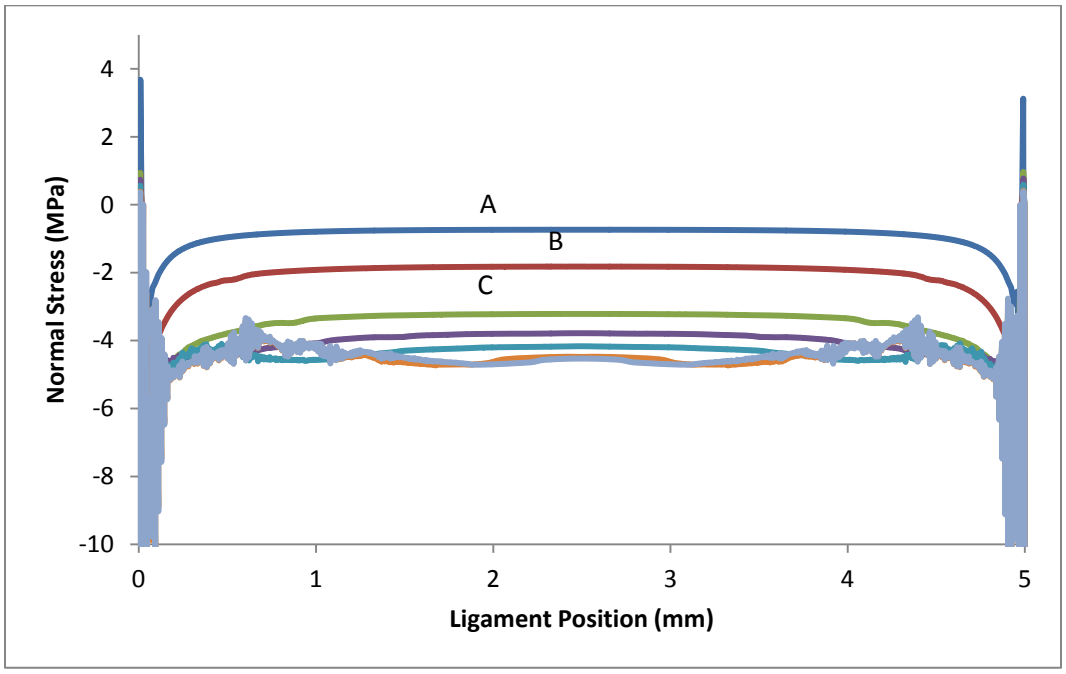

Figure 3.24: Ligament Normal Stress

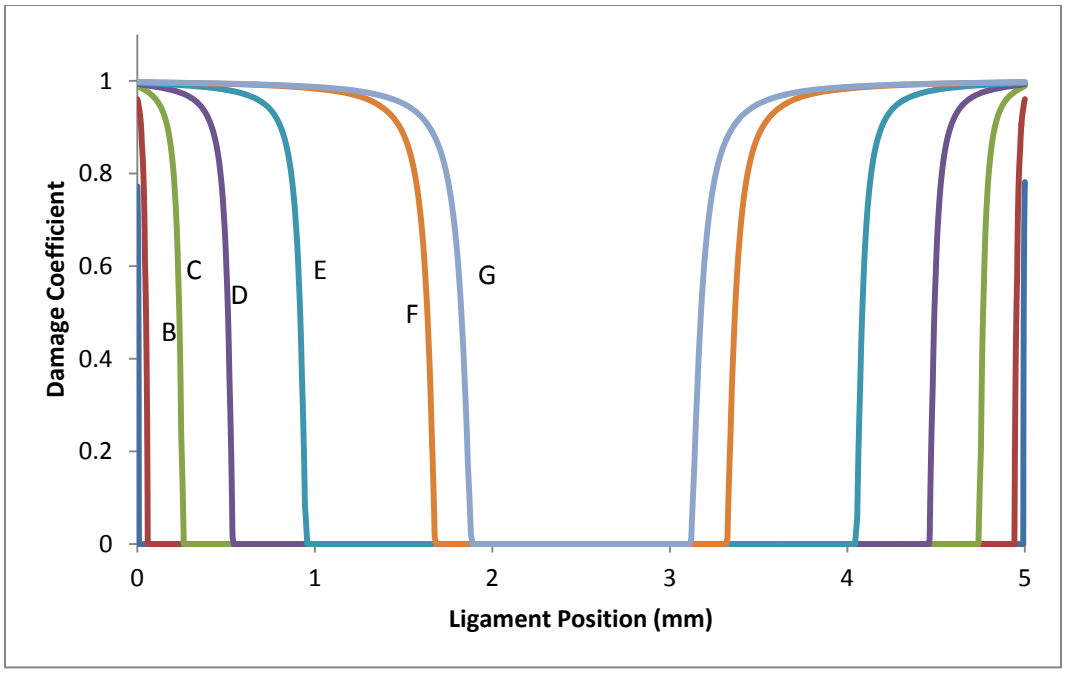

Figure 3.25: Damage Propagation

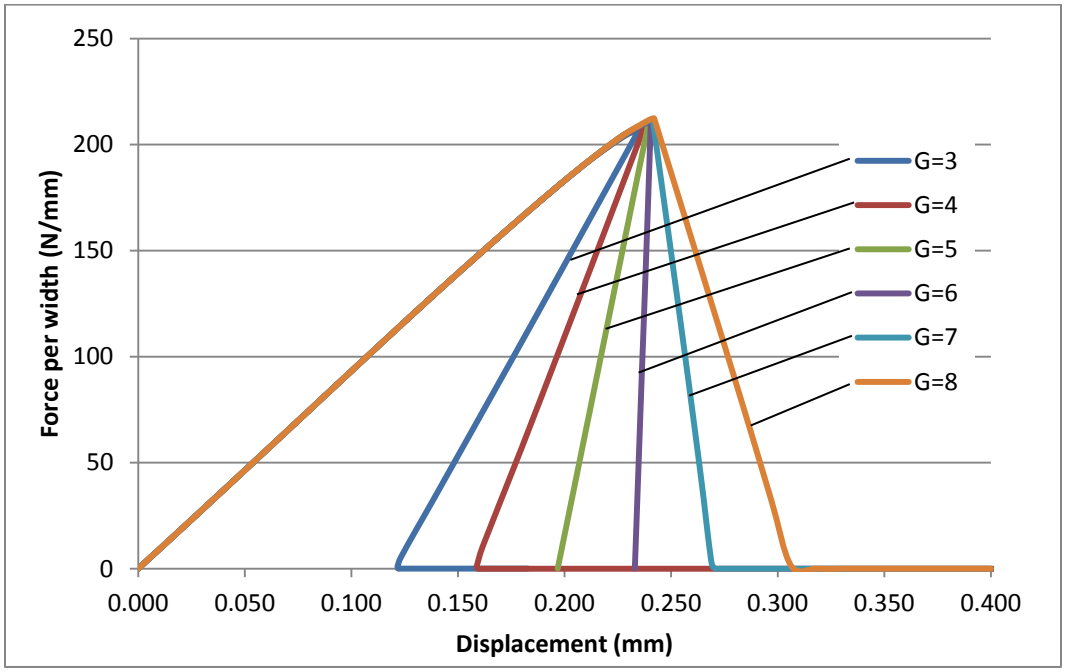

Figure 3.26: Transition to Stable Fracture

Chapter 4 - Discussion

Introduction

This chapter will discuss the implication of the results from the Iosipescu double edge notched shear (IDENS) test. The results and methodology in this work will be compared to the work of others to put it into the context of the larger body of knowledge for fracture mechanics.

Empirical Results

When compared with the fracture energy obtained from an ENF test, the IDENS test agrees with only one of the ENF measures defined by the ESIS protocol. The EWF from the Iosipescu DENS test is the same value as G_{IIc} if calculated from the nonlinear point, but lower than G_{IIc} if calculated from the maximum load. This difference might be explained by the relative size of the two specimens. The crack growth in a DENS specimen is limited to half the ligament length while the ENF specimen permits a long crack growth. The DENS specimen therefore expends very little energy growing the crack after damage initiation, so its energy at this point is similar to the energy at first damage initiation (nonlinear point) during an ENF test.

The energy release rate for the ENF test is calculated using an assumption of stable crack growth, even though the growth is unstable. Friction along the crack surface is also believed to increase the observed fracture toughness, but not substantially [42]. The EWF method tracks total energy without regard to its specific growth regime, which prevents problems related to calculating energy from multiple sources.

A softening in the load curve was seen after the ligament length was increased from 5 mm to 6 mm, which was attributed to buckling in the glass fibers. This identifies a size limit on the Iosipescu DENS specimen, after which a pure shear fracture can't be generated. The critical length of reinforcement fiber is a material property, dependent on the fiber/matrix system being studied, so it is possible that this method would be unable to generate enough data points to accurately determine the EWF of certain materials.

FEM Results

The material is neither isotropic nor ductile, but the SWF has a linear dependence on ligament length. The finite element model reveals that elastic strain energy is the dominant geometry dependent energy mechanism. The basic elliptical stress distribution is present near the ligament area, although it is elastic rather than plastic. Due to transverse isotropy, the microstructure changes only with out of plane position. Since the material properties do not change along the length of the fracture process zone, the usual, elliptical stress distribution occurs and will scale with ligament length. A glass/epoxy laminate is a brittle material with little plastic deformation, causing the change of SWF with ligament length to be driven by elastic strain energy instead of the usual plastic strain energy. Table 3.4 demonstrates that approximately 75% of external work is stored as strain energy. When this strain energy is released, the relatively low plastic energy consumption creates a linear increase in SWF, although Figure 3.18 demonstrates it does not increase as much. Since both the elastic and plastic energy content suitably scale with ligament length, this suggests that the EWF method can be applied to brittle materials, regardless of any plasticity they exhibit.

The EWF determined from the peak loads in the model is different than EWF determined from experiment. Although the model reproduces the results for ligament lengths 2-5 mm within the scatter in the experiment data, the EWF value from the peak loads is 0.95 kJ/m^2 instead of 2.18 kJ/m^2. Even when considering the EWF band in Figure 3.9, the peak loads from the model are not in agreement. The disagreement is explained in Figure 3.14 which shows the SWF move from the low end of the data scatter for 2 mm, to the high end of the data scatter for 5 mm. This is demonstrating a property of energy extrapolation methods: The results from these methods are extremely sensitive to variations in the collected data (scatter).

The original material property of 2.18 kJ/m^2 is calculated when the unstable crack growth curve is generated using the Riks arc length solution method, but not when calculated from the peak load values. This could be due to additional deformation mechanisms that were not modeled, such as a small nonlinearity in the elastic response. The elastic contribution to an increasing SWF would therefore be more material property dependent than the plastic contribution.

EWF Applied to Iosipescu DENS

In Chapter 1, ideal conditions were defined for the EWF method: full ligament yielding, self similar load-displacement curves, plane stress state, linear dependence of SWF on ligament length. Since these conditions were developed for mode I fracture in polymers and metals, they should be revisited for mode II fracture in the glass/epoxy composite studied here.

Full ligament yielding before the onset of fracture prevents excessive unloading in the plastic zone that is present for ductile materials. Unless plastic deformation energy dominates the region next to the fracture process zone, the method's governing energy partition is not met. Since a glass/epoxy composite is quasibrittle, elastic strain energy dominates. Also, full yielding before damage initiation does not occur because Figure 3.23 shows the ligament carries a higher stress at the current crack front than at its center. Since elastic strain energy and plastic deformation energy both scale appropriately with ligament length, their relative contribution does not need to be identified.

Self similar load curves for ductile materials are a way to check for changes in the deformation mechanisms: self similarity indicates the same mechanism. Average ligament stress at the failure point serves this function for the composite material. The average fracture stress was constant for ligament lengths 2-5 mm, indicating a brittle fracture with the same stress distribution. The lower fracture stress for the 6 mm ligament length, along with its lower stiffness, indicates that its stress distribution is different from the other sizes.

The original requirement for a plane stress state was to prevent the stress state from transitioning to plane strain at low ligament length (called a mixed mode failure). Since the new specimen is always under a state of plane strain, this condition is no longer required.

Comparison to Other Tests

The most popular tests for mode II interlaminar fracture toughness are the Edge Notched Flexure (ENF) and the End Loaded Split (ELS). Less popular methods include the Stabilized Edge Notched Flexure (SENF) and the Four Point End Notched Flexure (4ENF). These test procedures have the same options for the point from which to calculate G_{IIc} as the ENF does - maximum, nonlinear, 5% offset. All of these tests have proven themselves to be repeatable and consistent in round robin testing, provided G_{IIc} is calculated from the maximum load [10]. If the nonlinear point is used, then the ENF test gives a higher fracture energy than the others. The 5% offset point is usually the same as the maximum load point. For stable tests, the R-curve is also similar between these specimen configurations.

The ENF test was initially used for determining stress intensity factors in wood [43]. It was later adopted for interlaminar fracture in composites. A beam

theory approach for energy release rate in the ENF was proposed in 1988 by Williams [44]. This beam theory solution was presented as an alternative to energy based analytical methods and numerical methods. The easy analytical solution to the ENF and its convenient three point bending fixture have made it the most popular test method for Interlaminar fracture toughness. Despite its convenience, the ENF method has been criticized for not generating stable crack growth [9].

The ELS test was first introduced by Corletto at Texas A&M University in 1986 [45]. This test is preferred by the European Structural Integrity Society (ESIS) because it generates stable crack growth, which allows an R-curve to be found from a single test [9]. The ELS test is an end loaded cantilever beam supported by a clamp and roller combination fixture that allows sliding but not bending, although tests have been performed using a simple fixed clamp [42]. This fixture usually needs to be built into the loading frame so it is less popular than the ENF. In spite of being less popular than the ENF, a draft for standardization is currently being reviewed by the ISO [46].

The Japanese Industrial Standards Organization has included the SENF test in its standards for composite testing [47]. The SENF is a stabilized version of the three point ENF configuration that uses an instrumented specimen and a feedback control loop to prevent unstable crack growth. Such a control system is the physical equivalent of an arc length method. If the numerical results for unstable crack growth in the IDENS model were to be validated with experiments, the test configuration would resemble the SENF principle. This test is unpopular because of the instrumentation and control system requirement.

A four point bending version of the ENF specimen for mode II fracture was introduced by Martin and Davidson in 1999 [48]. The four point bending configuration maintains a constant bending moment between the inner loading pins. Like the ELS specimen, this specimen allows multiple compliance calibrations and an R-curve to be determined from a single test. The 4ENF test generally gives fracture toughness values that are similar to the ENF test [10] or slightly higher [42]. The difference in fracture toughness is thought to be from higher friction along the ENF crack surface [42].

There is uncertainty in the literature about what the critical point on the load curve is for the ENF test. The maximum load point or the nonlinear point are used for the calculation of G_{IIc} with the 5% offset point usually coinciding with the maximum load, as in the ENF test results presented here. The nonlinear point coincides with the visible onset of damage [49] in thermosets. Klabermatten et. al. used X-ray radiography to show the change to nonlinearity is caused by delamination at the beam's center, which may or may not be visible from the outside edges [50]. This result is not surprising, because the center is under a condition of plane strain. Since shear stress causes damage ahead of the

crack tip, further damage after crack initiation takes place in a damaged region that is not necessarily representative of the intrinsic material property.

The ENF and ELS specimens are sensitive to variations in thickness, whereas the DENS specimen was shown to be insensitive to thickness. Direct shear loading in the IDENS means that its compliance has a first order dependence on thickness. Due to the way the samples were built, insensitivity to thickness also means insensitivity to small changes in volume fraction, which can be supported by the finite element model. In the model, the effects of the crack are localized to the ligament area and first fiber layer, causing the rest of the specimen to not affect the fracture process zone.

Arc Length Methods

The first arc length method was proposed by Riks in 1972, who was trying to model unstable behavior after snap through and buckling [40]. A snap through problem is one in which equilibrium states don't exist for loads above a critical value, whereas a buckling problem is characterized by a bifurcation of equilibrium paths at a critical value [40]. In 1980, Crisfield adapted the approach taken by Riks for use in finite element procedures [41].

Arc length methods are used in fracture mechanics to simulate the snap back effect due to unloading during crack propagation. Unloading happens behind the cohesive zone in a quasibrittle material because its damage is much more localized than in a ductile material. Figure 3.26 demonstrates, unstable crack propagation phase can be removed by increasing the required fracture energy (effectively changing it from brittle to ductile).

The results in the present study agree with previous work in crack propagation. The method of beginning a simulation under displacement control in the stable regime and then switching to arc length control in the unstable regime was also followed by Távara et al [51]. Távara used cohesive elements in a Galerkin boundary element model to represent mode I fracture in a concrete SENB specimen. He observed the same apparent unloading behavior during unstable growth that was seen in the IDENS test. Like in the present work, the unstable load curves were steeper with a smaller crack (larger ligament length) and with lower fracture energy. An eventual stable crack growth was obtained if the cracks were long enough or the fracture energy was high enough. Távara's compared his results to a finite element method solution by Carpinteri and Colombo [52], who used a different cohesive model, and showed close agreement for his results.

Arc length methods are widely used in for cracks in concrete. Yang and Proverbs [53] compared 16 such arc length methods for crack propagation. They found that for an elastic damage model the snap back effect could only be captured by an arc length method, which could be either local or global, with local being more efficient. An example of local arc length method comes from Yang and Chen [54], who used an adaptive mesh in the growing fracture process zone. In their method, the mesh was refined near the crack tip and propagation was modeled as elements separating from each other by means of the crack opening displacement method. The arc length constraint was applied only to nodes within the refined zone, allowing an efficient and robust solution which was capable of tracking crack growth along an arbitrary and unknown path.

In 2003, Alfano and Crisfield introduced a double line search method for studying delamination in FRP [55]. They applied a scaling factor to both the load and displacement vectors (double line search) instead of only one of these parameters (single line search). In the event that the first line search failed, a unit value would be assumed and the second scaling parameter would be used. Near sharp corners in the solution, a single line search often requires an extremely small step size and may be unable to converge. By using the second line search, stability was improved in these regions.

Cohesive Elements

The cohesive zone model used for the ligament area is representative of current modeling practice. The advent of easy to implement cohesive elements in commercial finite element programs has led to their popularity in fracture and damage mechanics simulation. Cohesive elements are the current state of a continued effort to simulate realistic crack initiation and propagation. Two of the most sought after properties of a fracture simulation are ease of implementation and not requiring the crack path to be known a priori. These are the two criteria used here for evaluating a crack modeling techniques.

A popular technique from before standard cohesive elements were introduced is the virtual crack closure technique (VCCT). This is an intuitive model in which a crack was propagated by detaching adjacent elements from each other such that a mesh becomes two disconnected regions. The fracture energy is that which is required to virtually close the crack surfaces back to their original position. This technique had the advantage of easy mode partitioning and mixed mode calculation because displacements are readily available for every point on the crack surface. Pietropaoli and Riccio have done extensive work on interlaminar damage using VCCT that includes crack propagation [56], reduction in structure stiffness [57], and laminate buckling [57, 58]. This method is built on a straightforward principal, but it is mesh dependent and requires a known path.

More intensive algorithms have solved the a priori problem by using an adaptive mesh. Távara's model used a damage initiation criterion in all elements with an adaptive mesh at the crack tip to model crack growth [51]. By refining the mesh where it was needed, crack growth could be modeled along, arbitrary and unknown paths. Even though this technique did not require the path to be known, it was computationally expensive and still partially mesh dependent.

Cohesive models, like the one used in the Iosipescu DENS model, are governed by displacement discontinuity across an interface and a reduced stiffness. The linear softening model used here is the most common softening mode for cohesive elements; the next most popular being an exponential decay model. Bilinear and polynomial models are less popular.

Since simple cohesive elements have become part of the standard FEA toolkit, they can be independently studied. The cohesive elements in the IDENS finite element model are based on the recommendations of Turon's investigation of mesh size effects [39]. In this study, he developed the criterion in Equation 2.11, which sets the interface stiffness. Turon's criteria for the interface stiffness were that it be stiff enough to not add additional compliance to the model, but not so stiff as to cause stress oscillations. The compliance criterion represents the interface nature of a simple cohesive element: it is a numeric representation of surface cohesion, not actual material. The oscillation criterion addresses a numerical problem that can occur at a sudden change of stiffness, wherein surface tractions can oscillate along the interface as a result of Gaussian integration [59]. In this case, the stiff cohesive zone has a sudden change in traction across the nodes that divide substrate elements.

Compliant Tab Interface

The glued interface between the specimen and the aluminum tabs is unusually compliant, which increases the energy required to reach the fracture stress. Although this makes the SWF highly dependent on the glued interface, it does not change the EWF. Testing an uncracked specimen had a nonlinear force-displacement response, but its stiffness could be approximated as linear and it remained elastic. Thus, strain energy due to the glue stretching during a test is non essential work that disappears when the SWF is extrapolated back to an infinitely small ligament area.

Structural adhesives are problematic because they are usually more compliant than the materials they join. Their low stiffness is usually overcome by increasing the bonded area. With the specimen presented here, increasing the area to reduce interface compliance is not practical. The alternative to gluing mounting tabs onto a specimen is to use a larger, homogeneous version. If a V-notched beam like the one Gipple and Hoyns used [19] was created, its dimensions would be impractical. The material orientation required for

interlaminar shear requires length in the out of plane direction, ie laminate thickness. Since composite laminates are made from sheets (stitched fibers or pre-impregnated) it would require a very thick laminate. Figure 3.21 suggests that the required laminate thickness to replace the aluminum tabs would be 90mm.

Chapter 5 - Conclusions and Future Study

Conclusions

The Iosipescu DENS test, a new method for determining the mode II interlaminar fracture toughness of fiber reinforced polymers has been presented. This method has been investigated empirically and numerically, the results of which show this to be an accurate method.

The IDENS test is as accurate as the ENF test. When the measured EWF from the Iosipescu DENS test is compared with the G_{IIc} values from the ENF test, the two are in partial agreement. The average G_{IIc} when calculated from the nonlinear point is 2.45 kJ/m^2, while G_{IIc} is 3.55 kJ/m^2 when calculated from the maximum load. The average EWF calculated from the IDENS test is 2.18 kJ/m^2, while data scattering allows a range of 1.5-3.5 kJ/m^2. The ENF nonlinear point agrees strongly with the IDENS result, while the maximum load point is at the upper limit of possible EWF values. This is because the EWF calculated from the Iosipescu DENS test represents the crack initiation energy and damage initiates at the nonlinear point for the ENF test. The small ligament length for the DENS specimen doesn't permit a long cohesive zone, so the EWF represents initiation energy since very little crack growth happens after initiation.

The DENS specimen is insensitive to variations in its thickness. Over the range of 4.2-4.8 mm, the maximum load, and fracture displacement were independent of sample thickness. Tight thickness control is therefore not required for consistent results, making this specimen well suited for low precision layup techniques such as vacuum bagging. Thickness insensitivity also shows that the EWF is isolated from small changes in fiber volume fraction for the bulk material.

Brittle fracture causes elastic strain energy to replace plastic strain energy as the non-essential work of fracture. Since quasibrittle materials, such as the thermoset polymers used for a composite matrix, experience little plastic deformation before failure, they accumulate much less plastic strain energy than ductile materials. The plastic zone is also limited by the fiber layers on either side of the fracture process zone. Thus, instead of being eclipsed by plastic strain energy, elastic strain energy dominates the mechanical response. Further the transverse isotropic microstructure of FRP causes the strain energy to scale in a way amenable to the conventional EWF energy extrapolation.

The required conditions for the Essential Work of Fracture method are different for brittle materials using the DENS specimen in mode II, than for ductile materials using the DENT specimen in mode I. The requirements for the EWF method as applied here are less restrictive than the ones for ductile materials. 1) A plane strain stress state is required to prevent transition to a "mixed mode" failure. 2) A transverse orthotropic material is required for the SWF to have a linear dependence on ligament length.

Future Study

To continue investigating the Iosipescu DENS test as an alternative to the existing interlaminar fracture tests, there are a few directions that should be pursued.

One such direction would be to perform the test with other materials, such as a carbon fiber composite, in order to test their EWF compatibility. EWF compatibility in this case would include a linear increase in SWF with ligament length and require a brittle fracture. The test samples would also need to resist fiber buckling over enough ligament lengths to collect meaningful data.

Different adhesives should be compared in order to validate the finding that the adhesive stiffness does not affect the calculated EWF. Adhesives that yield or have a highly nonlinear response would likely be unsuitable.

A higher volume fraction glass/epoxy composite should be tested to determine the sensitivity to fiber dispersal. In the present study, the outer fiber layers were sparse, with a significantly lower fiber volume fraction than the inner layers. Although no significant phenomena occurred in the outer layers, the inner fiber bundles limited plastic deformation. Higher volume fractions lead to more uniform fiber distributions which could alter the deformation mechanisms.

Other directions could include a correlation study with other fracture toughness measures such as the stress intensity factor and J Integral.

References

[1] C. Hautamaki, S. Zurn, S. C. Mantell and D. L. Polla, "Experimental Evaluation of MEMS Strain Sensors Embedded in Composites," *Journal of Microelectromechanical Systems,* vol. 8, no. 3, September 1999.

[2] C. Ratcliffe, D. Heider, R. Crane, C. Krauthauser, M. K. Yoonb and J. W. Gillespie, "Investigation into the use of low cost MEMS accelerometers for vibration based damage detection," *Composite Structures,* vol. 82, p. 61–70, 2008.

[3] G. Zhou and L. M. Sim, "Damage detection and assessment in fibre-reinforced composite structures with embedded fibre optic sensors-review," *Smart Materials and Structures,* vol. 11, no. 6, p. 925–939, October 2002.

[4] M. D. Wood, X. Sun, L. Tong and Q. Luo, "A New ENF Test Specimen for the Mode II Delamination Toughness Testing of Stitched Woven CFRP Laminates," *Journal of Composite Materials,* vol. 41, no. 14, 2007.

[5] B. V. Sankar and S. K. Sharma, "Mode II delamination toughness of stitched graphite/epoxy textile composites," *Composites Science and Technology,* vol. 57, 1997.

[6] L. T. Tong and X. Sun, "Bending effect of through-thickness reinforcement rods on mode II delamination toughness of ENF specimen: Elastic and rigid–perfectly plastic analyses," *Composites Part A: Applied Science and Manufacturing,* vol. 38, no. 2, pp. 323-336, February 2007.

[7] T. K. O'Brien, "Composite Interlaminar Shear Fracture Toughness, GIIc: Shear Measurement or Sheer Myth?," *ASTM Special Technical Publication,* no. 1330, pp. 3-18, 1999.

[8] International Standards Organization, "15024 Determination of Mode I Interlaminar Fracture Toughness, GIC, for Unidirectionally Reinforced Materials," 2001.

[9] T. O'Brien, "Interlaminar fracture toughness: the long and winding road to standardization," *Composites Part B: Engineering,* vol. 29, no. 1, pp. 57-62, 1998.

[10] P. Davies, G. D. Sims, B. R. Blackman, A. J. Brunner, K. Kageyama, M. Hojo, K. Tanaka, G. Murri, C. Rousseau, B. Gieseke and R. H. Martin, "Comparison of Test Configurations for the Determination of GIIc: Results from an International Round Robin," *Plastics, Rubber an Composites,* vol. 28, no. 9, pp. 432-437, 1999.

[11] N. Iosipescu, "New accurate procedure for single shear testing of metals," *Journal of Metals,* vol. 2, no. 3, September 1967.

[12] D. E. Walrath and D. F. Adams, "The Iosipescu Shear Test as Applied to Composite Materials," *Experimental Mechanics,* vol. 23, no. 1, pp. 105-110, 1983.

[13] N. Conant and E. M. Odom, "An Improved Iosipescu Shear Test Fixture," *Journal of Composites Technology and Research,* vol. 17, no. 1, pp. 50-55, January 1995.

[14] D. F. Adams and D. E. Walrath, "Further Development of the Iosipescu Shear Test Method," *Experimental Mechanics,* vol. 27, no. 2, pp. 113-119, June 1987.

[15] American Society for Testing and Materials, "D 5379 Standard Test Method for Shear Properties of Composite Materials by the V-Notched Beam Method," 2005.

[16] G. W. Wycherley, A. Mestan and I. Grabovac, "A Method for Uniform Shear Stress-Strain Analysis of Adhesives," *Journal of Testing and Evaluation,* vol. 18, no. 3, pp. 203-209, May 1990.

[17] J. Morton, H. Ho, M. Y. Tsai and G. L. Farley, "An Evaluation of the Iosipescu Specimen for Composite Materials Shear Property Measurement," *Journal of Composite Materials,* vol. 26, no. 5, 1992.

[18] D. Adams and D. E. Walrath, "Current Status of the Iosipescu Shear Test Method," *Journal of Composite Materials,* vol. 21, June 1987.

[19] K. L. Gipple and D. Hoyns, "Measurement of the Out-of-Plane Shear Response of Thick Section Composite Materials Using the V-Notched Beam Specimen," *Journal of Composite Materials,* vol. 28, 1994.

[20] S. Lee, "Evaluation of Testing Techniques for the Iosipescu Shear Test for Advanced Composite Materials," *Journal of Composite Materials,* vol. 24, 1990.

[21] J. A. Barnes, M. Kumosa and D. Hull, "Theoretical and Experimental Evaluation of the Iosipescu Shear Test," *Composites Science and Technology,* vol. 28, pp. 251-268, 1987.

[22] I. Grabovac and C. E. Morris, "The Application of the Iosipescu Shear Test to Structural Adhesives," *Journal of Applied Polymer Science,* vol. 43, pp. 2033-2042, 1991.

[23] K. B. Broberg, "Critical review of some theories in fracture mechanics," *International Journal of Fracture,* 1968.

[24] Y. W. Mai, S. C. Wong and X. H. Chen, "Application of Fracture Mechanics For Characterization of Toughness of Polymer Blends," in *Polymer Blends: Formulations and Performance*, vol. 2, New York, Wiley, 2000, pp. 17-58.

[25] T. Bárány, T. Czigány and J. Karger-Kocsis, "Application of the essential work of fracture (EWF) concept for polymers, related blends and composites: A review," *Progress in Polymer Science,* vol. 35, no. 10, October 2010.

[26] H. J. Kwon and P. Y. Jar, "New Energy Partioning approach to the measurement of plane-strain fracture toughness of high density polyethylene based on the concept of essential work of fracture," *Engineering Fracture Mechanics,* vol. 74, no. 16, p. 2471–2480, 2007.

[27] H. J. Kwon and P. Y. Jar, "Fracture Toughness of Polymers in Shear Mode," *Polymer,* vol. 46, 2005.

[28] H. J. Kwon and P. Y. Jar, "Toughness of high-density polyethylene in shear fracture," *International Journal of Fracture,* vol. 145, p. 123–133, 2007.

[29] Y. W. Mai and B. Cotterell, "The Essential Work of Fracture for Tearing of Ductile Metals," *International Journal of Fracture,* vol. 24, pp. 229-236, 1984.

[30] J. S. Wong, D. Ferrer-Balas, R. K. Li, Y.-W. Mai, M. L. Maspoch and H.-J. Sue, "On Tearing of Ductile Polymer Films Using the Essential Work of Fracture (EWF) Method," *Acta Materialia,* vol. 51, pp. 4929-4938, 2003.

[31] Y. Hu, Z. Xia and F. Ellyin, "Deformation Behavior of an Epoxy Resin Subject to Multiaxial Loadings. Part 1: Experimental Investigation," *Polymer Engineering and Science,* vol. 43, no. 3, March 2003.

[32] European Structural Integrity Society, "Protocol for Interlaminar Fracture Testing of Composites," 1993.

[33] American Society for Testing and Materials, "D3171-11 Standard Test Methods for Constituent Content of Composite Materials," 2011.

[34] American Society for Testing and Materials, "D792-08 Standard Test Methods for Density and Specific Gravity (Relative Density) of Plastics by Displacement," 2008.

[35] American Society for Testing and Materials, "D2734-09 Standard Test Methods for Void Content of Reinforced Plastics," 2009.

[36] A. K. Kaw, Mechanics of Composite Materials, CRC Press, 1997.

[37] R. Hill, "A theory for the yielding and plastic flow of anisotropic metals," *Procedings of the Royal Society of London, Series A,* May 27, 1948.

[38] J. R. Davis, Surface Engineering for Corrosion and Wear Resistance, Maney Publishing, 2001.

[39] Dassault Systèmes Simulia Corp, "ABAQUS v6.9ef Documentation," 2009.

[40] D. Dugdale, "Yielding of steel sheets containing slits," *Journal of the Mechanics and,* vol. 8, pp. 100-104, 1960.

[41] G. Barenblatt, "The mathematical theory of equilibrium cracks in brittle fracture," *Advances in Applied Mechanics,* vol. 7, pp. 55-129, 1962.

[42] A. Turon, C. G. Dávila, P. P. Camanho and J. Costa, "An engineering solution for mesh size effects in the simulation of delamination using cohesive zone models," *Engineering Fracture Mechanics,* pp. 1665-1682, 2007.

[43] E. Riks, "An Incremental Approach to the Solution of Snapping and Buckling Problems," *International Journal of Solids and Structures,* vol. 15, pp. 529-551, 1979.

[44] M. A. Crisfield, "A Fast Incremental/Iterative Solution Procedure That Handles “Snap-Through”," *Computers and Structures,* vol. 13, pp. 55-62, 1980.

[45] W.-X. Wanga, M. Nakata, Y. Takao and T. Matsubara, "Experimental investigation on test methods for mode II interlaminar fracture testing of carbon fiber reinforced composites," *Composites: Part A,* vol. 40, p. 1447–1455, 2009.

[46] J. D. Barrett and R. O. Foschi, "Mode II Stress-Intensity Factors for Cracked Wood Beams," *Engineering Fracture Mechanics,* vol. 9, pp. 371-378, 1977.

[47] J. G. Williams, "On the calculation of energy release rates for cracked laminates," *International Journal of Fracture,* vol. 36, pp. 101-119, 1988.

[48] C. R. Corletto, "Mode II Delamination Fracture Toughness of Unidirectional Graphite/Epoxy Composites," MSc Thesis, Texas A&M University, 1986.

[49] International Organization for Standardization, "15114 Fibre-reinforced plastic composites — Determination of the mode II fracture resistance for unidirectionally reinforced materials using the calibrated end-loaded split (C-ELS) test and an effective crack length approach," 2012.

[50] Japanese Industrial Standards, "K7086 Testing Methods for Interlaminar Fracture Toughness of Carbon Fibre Reinforced Plastics," 1993.

[51] R. H. Martin and B. D. Davidson, "Mode II fracture toughness evaluation using four point bend, end notched flexure test," *Plastics, rubber, and composites processing and applications,* vol. 28, no. 8, pp. 401-406, 1999.

[52] R. H. Martin, "Interlaminar fracture characterization," *Key Engineering Materials,* Vols. 120-121, pp. 329-346, 1996.

[53] T. de Klabermatten, R. Jäggi, P. Flüeler, H. H. Kausch and P. Davies, "Microfocus radiography studies during mode I interlaminar fracture tests on composites," *Journal of Materials Science Letters,* vol. 11, pp. 543-546, 1992.

[54] L. Távara, V. Mantic, A. Salvadori, L. J. Gray and F. París, "SGBEM for cohesive cracks in homogeneous media," *Key Engineering Materials,* vol. 454, pp. 1-10, 2011.

[55] A. Carpinteri and G. Colombo, "Numerical Analysis of Catastrophic Softening Behaviour (snap-back instability)," *Computers and Structures,* vol. 31, no. 4, pp. 607-636, 1989.

[56] Z. J. Yang and D. Proverbs, "A comparative study of numerical solutions to non-linear discrete crack modelling of concrete beams involving sharp snap-back," *Engineering Fracture Mechanics,* vol. 71, pp. 81-105, 2001.

[57] Z. Yang and J. Chen, "Fully automatic modeling of cohesive discrete crack propagation in concrete beams using local arc-length methods," *International Journal of Solids and Structures,* vol. 41, p. 801–826, 2004.

[58] G. Alfano and M. A. Crisfield, "Solution strategies for the delamination analysis based on a combination of local-control arc-length and line searches," *International Journal of Numerical Methods in Engineering,* vol. 58, pp. 999-1048, 2003.

[59] A. Riccio and E. Pietropaoli, "Modeling Damage Propagation in Composite Plates with Embedded Delamination under Compressive Load," *Journal of Composite Materials,* vol. 42, no. 13, pp. 1309-1335, July 2008.

[60] E. Pietropaoli and A. Riccio, "A Global/Local Finite Element Approach for Predicting Interlaminar and Intralaminar Damage Evolution in Composite Stiffened Panels Under Compressive Load," *Applied Composite Materials,* vol. 18, no. 2, pp. 113-125, 2011.

[61] E. Pietropaoli and A. Riccio, "Finite Element Analysis of the Stability (Buckling and Post-Buckling) of Composite Laminated Structures: Well Established Procedures and Challenges," *Applied Composite Materials,* vol. 19, no. 1, pp. 79-96, 2012.

[62] J. C. Schellekens and R. de Borst, "A Non-Linear Finite Element Approach for the Analysis of mode-I Free Edge Delamination in Composites," *International Journal of Solid Structures,* vol. 30, no. 9, pp. 1239-1253, 1993.

[63] C. Schuecker and B. D. Davidson, "Evaluation of the accuracy of the four-point bend end-notched flexure test for mode II delamination toughness determination," *Composites Science and Technology,* vol. 60, pp. 2137-2146, 2000.